(2)

DEPARTMENT OF MATERIALS SCIENCE AND MINERAL ENGINEERING

INTERPRETATION OF AEM DATA IN TERMS OF ICE KEEL GEOMETRY

Final Report
prepared for NORDA
Under U.S. Navy contract #N00014-89-6004

by
G. Liu and A. Becker

Engineering Geoscience
August 1989

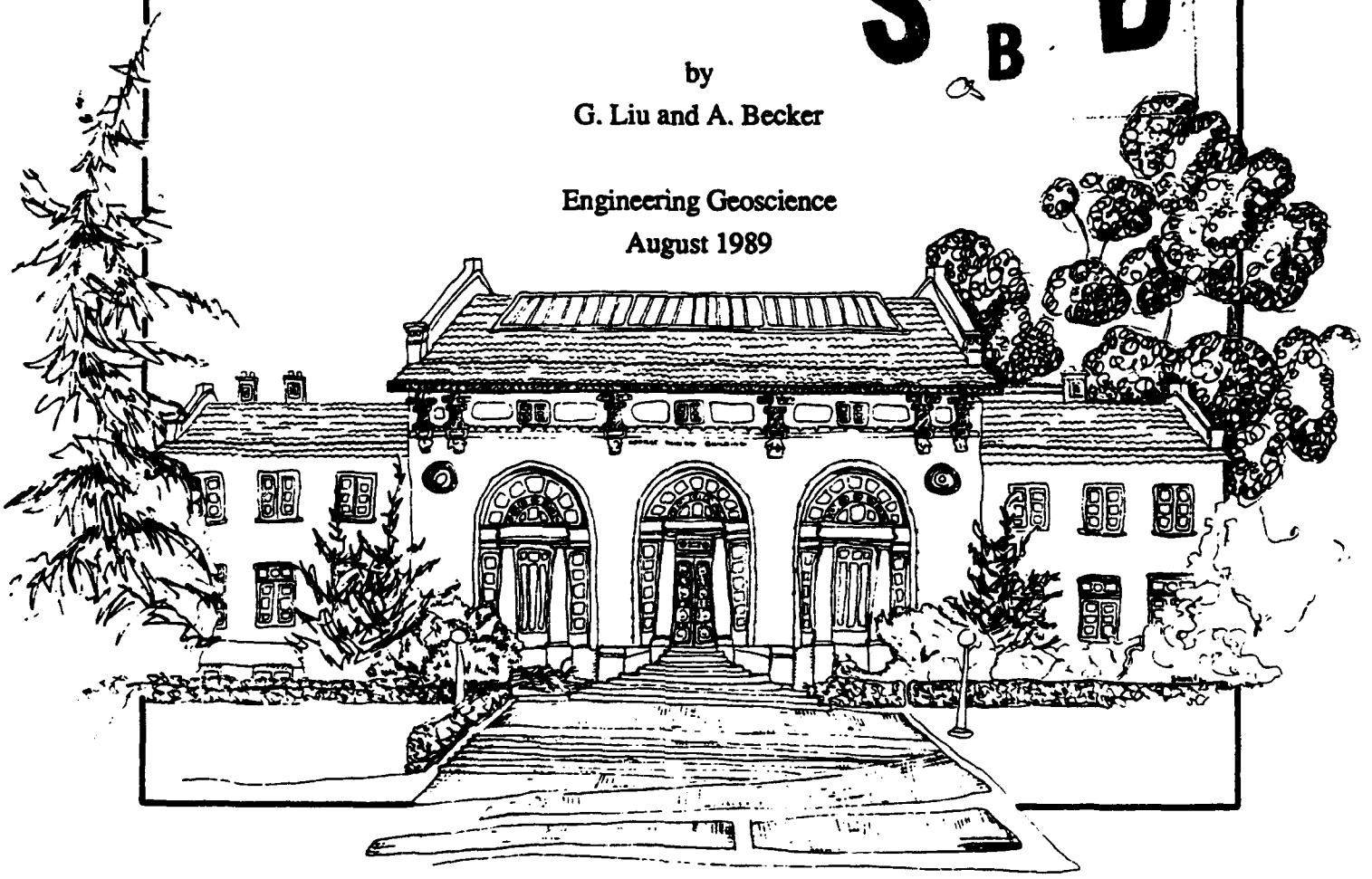

Hearst Mining Building
University of California, Berkeley

REPORT DOCUMENTATION PAGE

Form Approved
OMB No. 0704-0188

1. Agency Use Only *(Leave blank)*.	2. Report Date.	3. Report Type and Dates Covered.
	August 1989	Final August 1989

4. Title and Subtitle.
Interpretation of AEM Data In Terms of Ice Keels Geometry

5. Funding Numbers.
Program Element No. 63704
Project No. EV1299
Task No. 300
Accession No. DN257087

6. Author(s).
G. Liu and A. Becker

7. Performing Organization Name(s) and Address(es).
University of California, Berkeley
Dept. of Materials Science and Mineral Engineering
Hearst Mining Bldg.
Berkeley, CA 94720

8. Performing Organization Report Number.
CR N00014-89-K-6004

9. Sponsoring/Monitoring Agency Name(s) and Address(es).
Naval Ocean Research and Development Activity
Code 311
SSC, MS 39529-5004

10. Sponsoring/Monitoring Agency Report Number.

11. Supplementary Notes.

12a. Distribution/Availability Statement.
Approved for public release; distribution is unlimited.

12b. Distribution Code.

13. Abstract *(Maximum 200 words).*

A 2-Dimensional Occam inversion technique is applied to a Limited Airborne Electromagnetic (AEM) survey data set in order to verify that the theoretical expectations for ice keel parameter recovery can be met. Additionally, the data are corrected for aircraft altitude. The results showed a datum altitude correction can be successfully applied to AEM data. The 2-D inversion of the data was able to verify that ice keel geometry can be recovered from the data however, the method still requires extensive off-line processing.

for ice

14. Subject Terms.
snow, ice, and permafrost, dynamical oceanography, magnetic induction, electromagnetic pulses, physical oceanography, TOPOGRAPHY, WATER, INTERFACES

15. Number of Pages. 50

16. Price Code.

17. Security Classification of Report.	18. Security Classification of This Page.	19. Security Classification of Abstract.	20. Limitation of Abstract.
Unclassified	Unclassified	Unclassified	

NSN 7540-01-280-5500

Standard Form 298 (Rev. 2-89)
Prescribed by ANSI Std. Z39-18
298-102

Interpretation of AEM data
In terms of ice keel geometry

by

Guimin Liu and Alex Becker

INTRODUCTION

This study is a demonstration of the methods developed earlier (Becker and Liu, 1988) for the interpretation of AEM data in terms of ice keel geometry. The data were collected in Prudhoe Bay, Alaska by CRREL in 1987 (Kovacs and Holladay, 1989). The AEM system used in this survey was a down-sized version of the conventional system. It consisted of three coil pairs installed in a "bird" 3.5 meters long so that the separation between the transmiting and receiving coils was three meters. Two coil pairs operated in the co-planar mode at 811 Hz and 50 kHz while the other coil pair operated in the co-axial mode at 4.5 kHz. Here we will interpret the data acquired on lines F14L3 and F11L0 which were over a first-year ridge, and F13L8 which was over a multi-year ice floe (floe 3). These data are shown in Figures 1, 2 and 3 respectively, together with the bird height above the ice surface measured by a laser altimeter. They were previously interpreted using a one-dimensional (1-D) technique and it was noted that the ice thickness obtained in the areas of ice keels was seriously in error (Kovacs and Holladay, 1989). Assuming that the ice keels can be considered as two-dimensional, we will use chart interpretation and data inversion (Becker and Liu, 1988) to define the ice keels.

To verify the ice thickness determined by the AEM method, drill-hole measurements were made on a rectangular grid laid out at the the first-year ridge and on the multi-year ice floe (Kovacs and Holladay, 1989). The grid width was 50 m. The grid lengths were 225 m for the first-year ridge and 200 m for the multi-year ice floe. The grid points were spaced 5 m in each direction. At each grid point the snow and ice thickness was determined, and so were the free-board and keel depths. The AEM system was flown down the center of each grid and the measurements were referred to the location of the station markers placed at 25 m intervals on the ice surface. Common fiducial numbers recorded on the AEM data and the flight path video allowed for cross correlation of the AEM data with the ice station location. For F14L3 the ten station markers on the ice correspond to the fiducials 3063, 3067, 3071, 3076, 3081, 3085, 3091, 3094, 3098, and 3102. For F11L0 the ten station markers on the ice correspond to fiducials 594, 596, 597, 599, 600, 601, 603, 604, 605, and 606. For F13L8 the nine station markers correspond to fiducials 5398, 5400, 5402, 5404, 5406, 5408, 5410, 5412, and 5414. Each fiducial interval corresponds to one second in time.

Prior to the chart interpretation of the data, a altitude correction is applied since the bird height varied significantly during a flight. That is, the data is first corrected to a datum, which is necessary before using the chart interpretation. For data inversion, this altitude correction is not absolutely needed but, as will be shown here, is desirable.

ALTITUDE CORRECTION

The altitude correction of the data is performed using the principle of complex images (Thomson and Weaver, 1975). It is well known that when a magnetic dipole excites a conductive ground, the secondary EM field in the air can be approximately calculated from an image dipole located at a complex depth at $h + \delta - i\delta$, where h is the height of the source over the ground, $i = \sqrt{-1}$, and δ is the skin depth of the EM wave,

$$\delta = \frac{503}{\sqrt{\sigma f}} \qquad (1)$$

Here σ is the conductivity of the ground and f is the operation frequency. The so-calculated field is accurate when the skin depth is much smaller than the height h or the transmitter-receiver separation (Thomson and Weaver, 1975). In our case, sea ice is quite resistive and its effects may be neglected. The skin depths of the EM wave in sea water at 50 kHz, 4.5 kHz, and 811 Hz are 1.4 m, 4.7m, and 11 m respectively. The skin depths at 50 kHz and 4.5 kHz are much smaller than the normal bird height of 25 m and the secondary magnetic field computed from the complex image is very accurate. For the 811 Hz data however, the calculated secondary magnetic field is accurate to within 1.5% for the in-phase component and 6.5% for the quadrature component. The error increases with decreasing the bird altitude.

Now suppose that one co-axial data d, which is the secondary magnetic field normalized by the primary magnetic field at the

receiver, is collected at a height z above the ice surface and we want to correct it to the datum z_0. Assume that the complex image is located at $h + \delta - i\delta$ below the ice-water interface. Note that δ is known since the operation frequency is given and the sea water conductivity can be assumed or calculated using a 1-D technique. Let s denote the distance between the transmitter and the receiver, then the computed data is,

$$c = \frac{s^3[2s^2-(2h+\delta-i\delta)^2]}{2[s^2+(2h+\delta-i\delta)^2]^{5/2}} \qquad (2)$$

In principle, h may be found by solving the equation d=c. In practice however, such a solution may not be possible due to model constraints. Instead, the solution that minimizes the difference d-c is sought. Once h is known, the normalized secondary magnetic field at the datum z_0 can be calculated from an image located at the complex depth $h+z-z_0 + \delta - i\delta$. The corrected data at datum z_0 is,

$$d' = \frac{s^3[2s^2-(2h+2z_0-2z+\delta-i\delta)^2]}{2[s^2+(2h+2z_0-2z+\delta-i\delta)^2]^{5/2}} \qquad (3)$$

For the co-planar coil configuration, equations (2) and (3) become

$$c = \frac{s^3[2(2h+\delta-i\delta)^2 - s^2]}{[s^2+(2h+\delta-i\delta)^2]^{5/2}} \qquad (4)$$

and

$$d' = \frac{s^3[2(2h+2z_0-2z+\delta-i\delta)^2 - s^2]}{[s^2+(2h+2z_0-2z+\delta-i\delta)^2]^{5/2}} \qquad (5)$$

The altitude-corrected data are shown in Figures 4, 5, and 6 for F14L3, F11L0 and F13L8 respectively. An ice keel is clearly indicated in Figure 4 at fiducials 3066-3080, in Figure 5 at fiducials 595-602, and in Figure 6 at fiducials 5398-5414. Note that the obvious altitude variation in the laser altimeter profile caused by the associated ice ridge is taken out before applying the altitude correction. Otherwise, the anomaly in the corrected data would be larger and sharper. In areas of level ice, the data plot after altitude correction should form a straight flat line for either the in-phase or quadrature component and its accuracy depends only on the validity of the complex image approximation. The ripples in the corrected data away from the ice keel in Figures 4 and 5 are probably caused by the noise in the altimeter readings. They correspond to an ice thickness variation of ± 20 cm except in areas of rapid changes of the altitude.

Here we also include an example of the altitude correction to the data collected over open sea water and an ice lead in Prudhoe Bay in 1985 by CRREL (Kovacs, et al., 1987). The AEM system used in this survey consisted of four coil pairs, two of which operated in the co-axial mode at 930 Hz and 4160 Hz while the other two operated in the co-planar mode at 530 Hz and 16290 Hz. The separation of the transmitter and receiver in each coil configuration is 6.45m. The original data on line F6L6 is shown in Figure 6(a) while the altitude-corrected data is shown in Figure 6(b). Clearly the data after altitude correction forms, except for some noise, a constant straight line over the open sea water to the right of fiducial point 3260. A one-dimensional interpretation shows zero ice thickness in this area. To

the left of fiducial point 3260, the AEM response is smaller. This corresponds to an ice lead about 65 cm thick. Note that a 17 ppm change is observed in the in-phase component of the 4160 Hz data to the left of fiducial point 3260 while a 25 ppm change at 34m altitude corresponds to 1 m thick sea ice. The error of the altitude correction is largest for the 530 Hz data, which is less than 1% for the in-phase component and 5.6% for the quadrature at h = 34m. Errors of the altitude correction for data at other frequencies can be neglected.

CHART INTERPRETATION

First we construct a chart that relates the parameters of the anomaly in the system response to the geometrical variables of the associated ice keel. The model ice keel is chosen to have a Gaussian shape (Becker and Liu, 1988) whose draft is given by

$$t(x) = A \exp\left(-\frac{x^2}{0.361\, W^2}\right) \qquad (6)$$

Here,

x = distance from the keel center line

A = maximum keel draft

W = keel width at half maximum draft

The shape of the keel is invariant along its strike direction (y direction). The associated AEM anomaly is characterized by the two parameters "normalized anomaly amplitude", which is the anomaly amplitude normalized by the background response, and the "normalized anomaly width", which is the anomaly width normalized by the average bird height above the sea-water surface (Becker and

Liu, 1988). An example illustrating these parameters is given in Figure 7.

We used the algorithm developed earlier (Becker and Liu, 1988) for rapidly computing the AEM response in the inductive limit. By compiling numerical results for a variety of ice keel models, we constructed an interpretation chart for each of the coil configurations. The charts for the co-axial and co-planar system anomalies are shown in Figures 8 and 9. The charts are constructed for a bird height of h=20 m over the ice-water interface. The abscissa in the chart is the normalized anomaly width while the ordinate is the normalized anomaly amplitude. The solid lines in the chart are for constant keel draft A and the dashed lines are for constant keel width W. The displayed values a and w are the values of A and W normalized by the norminal bird height h. Thus from an observed AEM anomaly we can obtain its normalized width and amplitude and plot these parameters on the chart. The normalized keel width and draft can then be read off the chart.

Now let us interpret the system anomalies on lines F14L3 and F11L0 in Figures 4 and 5. Since the charts are constructed using numerical results in the inductive limit, we need to add the in-phase and quadrature components before interpretation (Liu, 1989). The anomaly parameters are then obtained from this sum profile. Figure 10 shows an example of the sum profile for F14L3. The distance shown on the abscissa is obtained from the two fiducials corresponding to the station markers at the ends of the grid on the ice. Flight speed is assumed to be constant over the grid. The

measured anomaly parameters are listed in Table 1. Points p_3 and p_4 on Figure 9 correspond to the anomalies in the 811 Hz and 50 kHz data; point p_1 on Figure 8 is for the 4.5 kHz data. The values of the normalized keel width and keel draft read off the charts are also listed in Table 1. The interpreted values of the normalized keel width obtained from different frequencies agree within ± 6.6% with an average value of 1.06 (21.73 m). Those values of the normalized keel draft agree within ± 12% with an average value of 0.43. Note the large difference between the keel parameters interpreted from the 811 Hz and 50 kHz data recorded with the same co-planar coil configuration. The interpreted keel from the 811 Hz data is much larger than that obtained from the 50 kHz data. Theoretically however, the interpreted keel using the higher frequency data should be a little larger (Liu, 1989). The contradictory observation suggests that the first-year keel may have a wet zone at the ice-water interface. This wet zone was actually detected by drill-hole measurements (Kovacs and Holladay, 1989).

The interpreted keel using the 4.5 kHz data is plotted in Figure 11 together with the drill-hole data (averaged over 11 adjacent lines). The associated ridge is obtained by subtracting the smoothed altitude from the altimeter readings. The interpreted keel is somewhat smaller than the drill-hole meassurements. Its peak is 3.5 m too shallow.

For the data on line F11L0, the anomaly parameters and the keel variables are listed in Table 2. Points p_5 and p_6 on Figure 9 correspond to the 811 kHz and 50 kHz data; point p_2 on Figure 8

corresponds to the 4.5 kHz data. The interpreted keel from the 4.5 kHz data is plotted in Figure 12. It is seen that the interpreted keel is much smaller than the drill-hole measurements. It is also much shallower and wider than the interpreted keel obtained from the F14L3 data. Moreover the keel peak is delayed by 20 m in the flight direction in this case. The fact that the interpreted keel is much shallower and wider and is delayed in time may be caused by the time constant of the instrument channels. The system anomaly is a convolution of the static anomaly with the impulse response of the instrument (Becker and Cheng, 1987). Thus the anomaly is delayed and flattened in the record. If the time constant of the instrument is small or the instrument moves slowly over the target, the effects of the distortion may be neglected. This is probably the case for line F14L3. In recording line F11L0 however, the helicopter flew at a speed more than three times faster than that in F14L3. It appears that the time constant of the instrument did not allow the static anomaly to be fully expressed, which resulted in a delayed shallower and wider keel. Note that the interpreted keel from the 50 kHz data is smaller than that from the 811 Hz data. This is consistent with the F14L3 data interpretation.

Part of the 20 m delay in the interpreted keel may be caused by the inaccuracy of the recording of the manual ticks corresponding to the station markers on the ice surface. Since the 225 m grid was flown over in 12 seconds, one fiducial interval corresponds to 19 m in distance. The discretization error of half a fiducial in placing the manual ticks is 9.5 m. The fiducials corresponding to station markers

show abrupt changes of flight speed which are not possible. Hence we only used the two fiducials corresponding to the ends of the grid laid out on the ice surface and assumed a constant flight speed.

For data on line F13L8 over the multi-year ice floe, the anomaly parameters and the interpreted keel variables are shown in Table 3. In this case only the anomaly on the 50 kHz data is interpreted. The keel variables are the average values of those interpreted from charts constructed for h=20m and h=25m since h is actually 22.6m in this case. Point p_7 in Figure 9 and 9(a) shows the corresponding point for the anomaly in each chart. The points for the 811 Hz and 4.5 kHz data are far off the chart for h=25m and can not be extrapolated accurately for interpretation. The interpreted keel from the 50 kHz data is shown in Figure 13. It agrees well with the drill hole measurements.

INVERSION

The objective of the inversion algorithm is to find the smoothest ice keel that fits the data within a specified tolerance. It does not require the keel to have a prescribed shape. Since it is designed for data acquired in the inductive limit, the sum of the in-phase and quadrature needs to be scaled to approximate the required data for inversion (Liu, 1989). The scale factor is the ratio of the inductive limit response to the lower frequency response at the datum flight height.

The co-axial 4.5 kHz scaled data (scale factor = 1.114 at h = 20.5 m) is shown in upper Figure 14 (thick line). The inverted keel is

shown in lower Figure 14 (thin line) while the drill-hole measurements are shown by the thick line. In the inversion the end points of the unknown section of the ice-water interface are fixed at 30 m and 118 m respectively. A four meter sampling interval is used to discretize the ice-water interface. This sampling interval is used in all the cases studied here. The level ice thickness is fixed at 1.5 m to the left of the ice keel and at 2.3 m to the right as indicated by the 1-D interpretation results. 27 data points from fiducials 3065 to 3091 are used. The upper part of the keel is defined quite well from the data inversion (fourth iteration with an average misfit of 5 ppm per data point) even though it is somewhat shallower than the drill-hole measurements. The maximum ice thickness recovered from the inversion is 13.5 m which is identical to that obtained from the chart interpretation. This value is 4 m smaller than the drill-hole measurement. For the same case, the 1-D interpretation gives a maximum of 10 m (Kovacs and Holladay, 1989). The fact that the keel peak was not recovered from the data inversion may be caused by two factors: (1) the keel peak was wet and there was not a sharp electric boundary between the ice and the water; (2) the scheme of smooth inversion did not allow a sharp peak to be reconstructed (Becker and Liu, 1988).

The co-planar 50 kHz data set which is scaled by a factor of 1.012 at h=20.5 m, is also inverted and the results are shown in Figure 15. Conditions for the inversion are identical to those in the above case. The inverted maximum keel draft is the same as the result shown in Figure 14 while the keel width is apparently smaller.

Since the inversion algorithm can be applied to data acquired at a variable flight height, the 4.5 kHz data is also inverted before the altitude correction. The sum of the in-phase and quadrature is scaled by a factor of 1.134 which corresponds to a bird height of 19 m above ice-water interface. The inversion results are shown in Figure 16. The inverted keel is one meter shallower than the one shown in Figure 14. Moreover, the misfit at the left part of the data is large. This is probably caused by the constant scale factor which is too large for this part of the data. Note also that the position of the two end points of the unknown section are not obvious in the original data. Here they were fixed at the position obtained from the altitude corrected data. From this test analysis it appears that it is advantageous to apply the altitude correction before doing the inversion.

The inversion of the 4.5 kHz altitude-corrected data on line F11L0 is shown in Figure 17. In this case, 13 data points from fiducials 594 to 606 are used and 23 unknowns are sought. The end points are fixed at 46 m and 134 m respectively. The level ice thickness is fixed at 1.5 m at the left and right hand sides of the keel. The inverted keel is much smaller than the drill-hole measurements and it is also much smaller than the interpreted keel from the 4.5 kHz data on line F14L3. Moreover, just as for the chart interpretation the interpreted keel is shifted in the flight direction.

The last data set that is inverted is the 50 kHz co-planar data (scale factor = 1.010 at h = 22.6 m) over a multi-year keel. 14 data

points from fiducials 5401 to 5414 are used to solve for 28 unknowns. The ends of the unknown section of the ice-water interface are fixed at 78 m and 186 m in this case. The level ice thickness at left and right sides of the keel are 3.6 meters. The results of the data inversion are shown in Figure 18. If we ignore the sharp peak, the interpreted keel shape is quite close to its true form.

SUMMARY

(1) A datum altitude correction can be successfully applied to AEM data. After this correction the data clearly indicates the topography of the ice-water interface. This correction is necessary before using the chart interpretation. Moreover, even for data inversion, it is advantageous to use the altitude-corrected data.

(2) The chart interpretation and the inversion for the data on line F14L3 yield identical maximum ice thickness over the first-year ridge. Data inversion also correctly defines the upper part of the ice keel. The keel peak however, is 4 m smaller than the drill-hole measurement. This may be caused by three factors: (1) the keel peak was wet and there was not a sharp electric boundary between the ice and the water; (2) the scheme of smooth inversion did not allow a sharp peak to be reconstructed; (3) the time constant of the instrument did not allow a full expression of the AEM static anomaly for the ice keel.

(3) In F11L0, because of the time constant of an instrument channel the fast flight speed distorted the anomaly shape so that the interpreted keel is much smaller. Moreover it delays the anomaly in

the flight direction. To solve this kind of problem, the time constant of the instrument should be made smaller or the helicopter should fly more slowly.

(4) For the data on line F13L8 over a multi-year ice keel, both chart interpretation and data inversion yield results close to the drill-hole measurements.

REFERENCES

Becker, A., and Cheng, G., 1987, Detection of repetitive electromagnetic signals, in Nabighian, M. N. Ed., Electromagnetic methods in applied geophysics - theory, Vol. 1.

Becker, A., Liu, G., 1988, Airborne electromagnetic Mapping of Sea-ice Keels, Report prepared for NORDA under UCB contract #N00014-87-K-6005.

Kovacs, A., and Holladay, J. S., 1989, Airborne sea ice thickness measurement system development and field test results, Report prepared for NORDA.

Kovacs, A., Valleau, N., and Holladay, J.S., 1987, Ariborne electromagnetic sounding of sea-ice thickness and sub-ice bathemetry: Cold Regions Science and Technology, vol.14, 289-311.

Liu, G., 1989, Airborne electromagnetic sensing of sea ice thickness, Ph.D thesis, Univ. of California at Berkeley.

Thomson, D. J., and Weaver, J. T., 1975, The complex image approximation for induction in a multilayered earth: J. Geophy. Res., vol. 80, 123-129.

Table 1. Observed anomaly parameters for F14L3 and Corresponding interpreted keel parameters

h=20.5 m

	normalized anomaly		normalized keel			
Frequency	amp.	width	draft	width	interpreted draft (m)	actual draft (m)
811 Hz	0.50	2.66	0.45	1.13	9.2	12.7
4.5 kHz	0.51	2.16	0.45	1.06	9.2	12.7
50 kHz	0.43	2.43	0.38	0.99	7.8	12.7

Table 2. Observed anomaly parameters for F11L0 and Corresponding interpreted keel parameters

h=20.5 m

	normalized anomaly		normalized keel			
Frequency	amp.	width	draft	width	interpreted draft (m)	actual draft (m)
811 Hz	0.44	3.53	0.23	2.02	4.7	12.7
4.5 kHz	0.41	3.00	0.22	1.76	4.5	12.7
50 kHz	0.37	3.36	0.18	1.97	3.7	12.7

Table 3. Observed anomaly parameters for F13L8 and Corresponding interpreted keel parameters

h=22.6 m

	normalized anomaly		normalized keel			
Frequency	amp.	width	draft	width	interpreted draft (m)	actual draft (m)
811 Hz	0.25	3.82	-	-		
4.5 kHz	0.27	3.90	-	-		
50 kHz	0.27	3.39	0.13	2.37	2.9	3.4

TABLE OF ILLUSTRATIONS

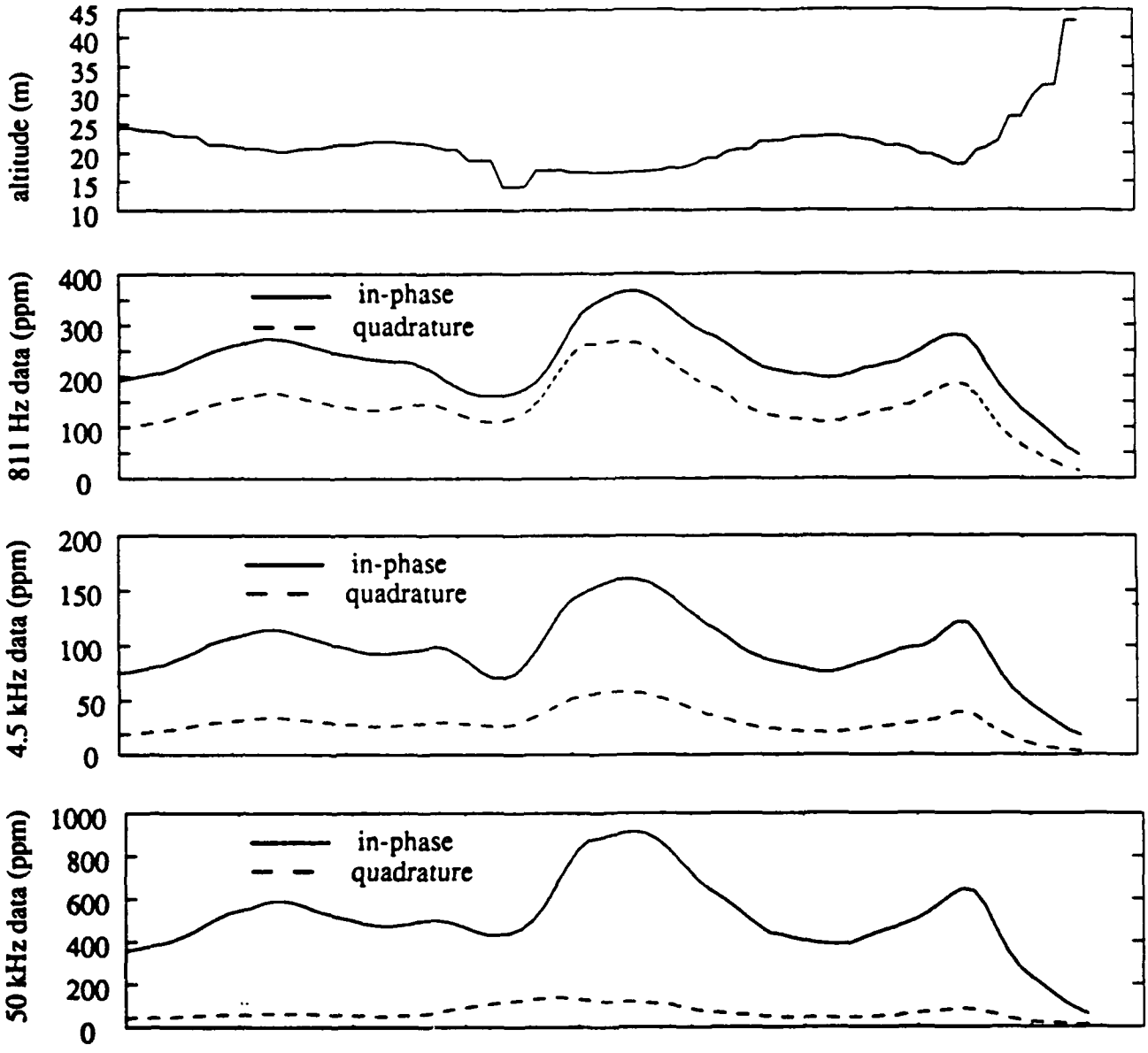

Figure 1. Data on line F14L3; Fiducials 3063-3098.

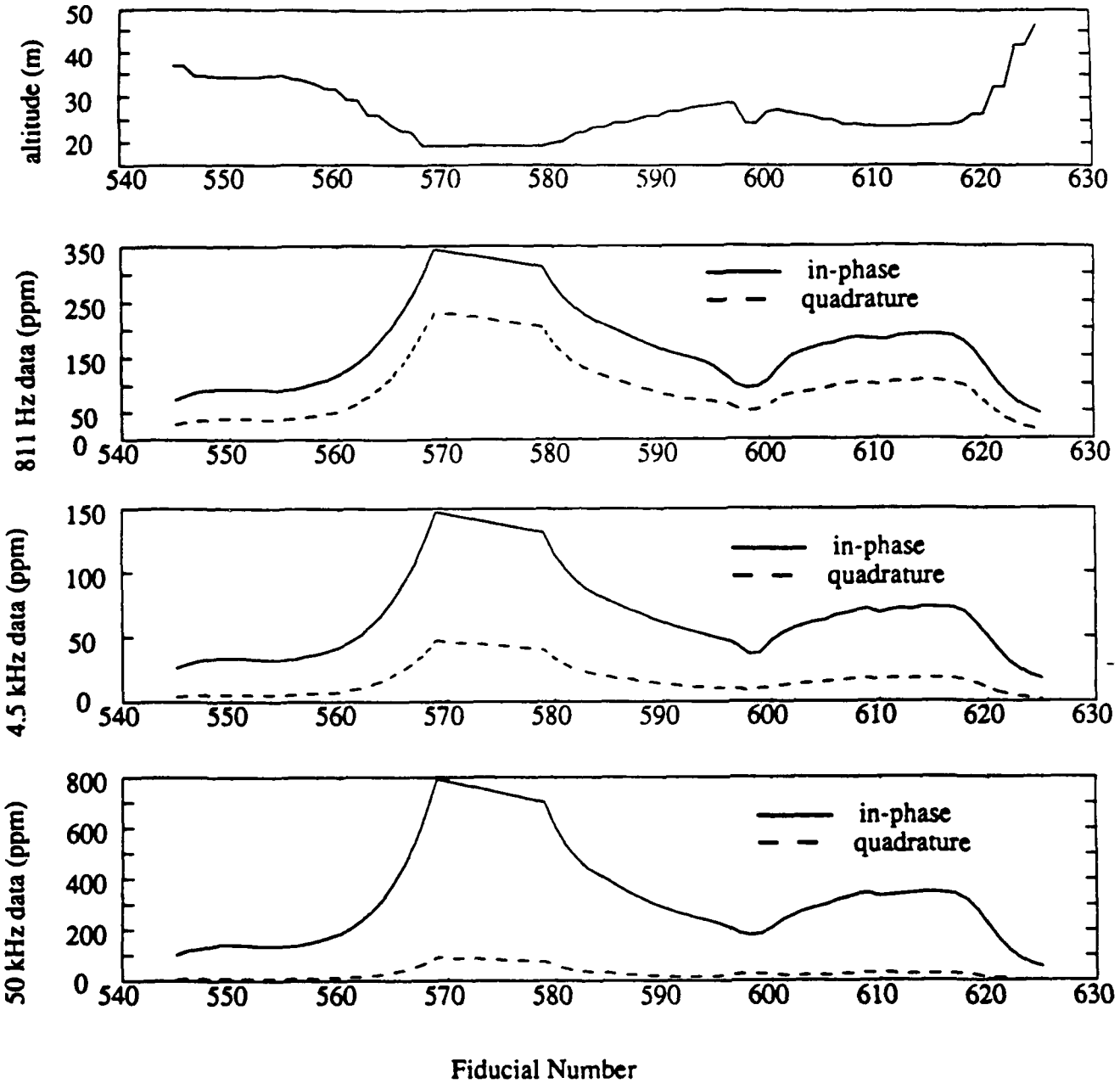

Figure 2. Data on line F11L0; Fiducials 594-606.

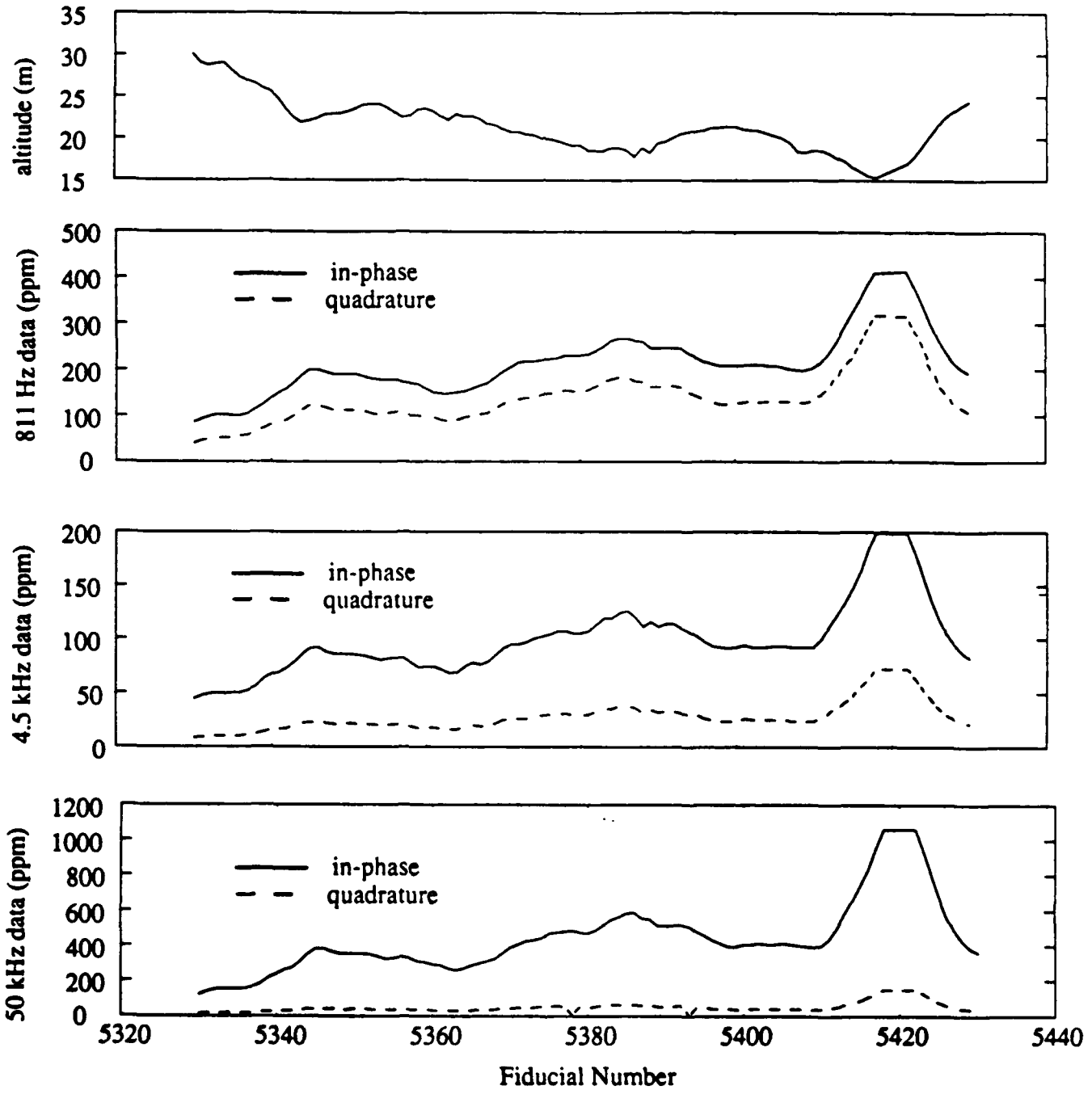

Figure 3. Data on line F13L8; Fiducials 5398-5414.

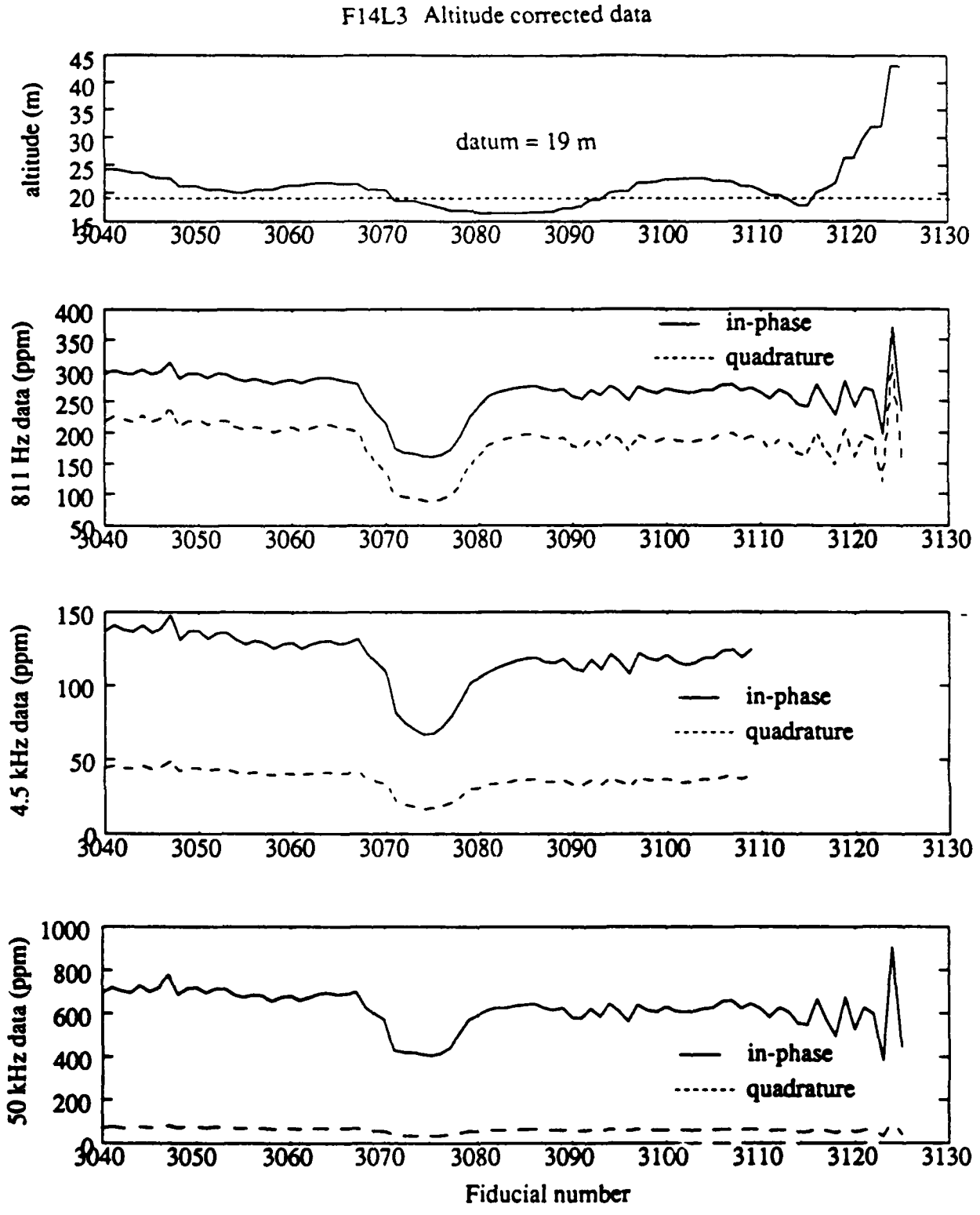

Figure 4. Altitude-corrected data on line F14L3.

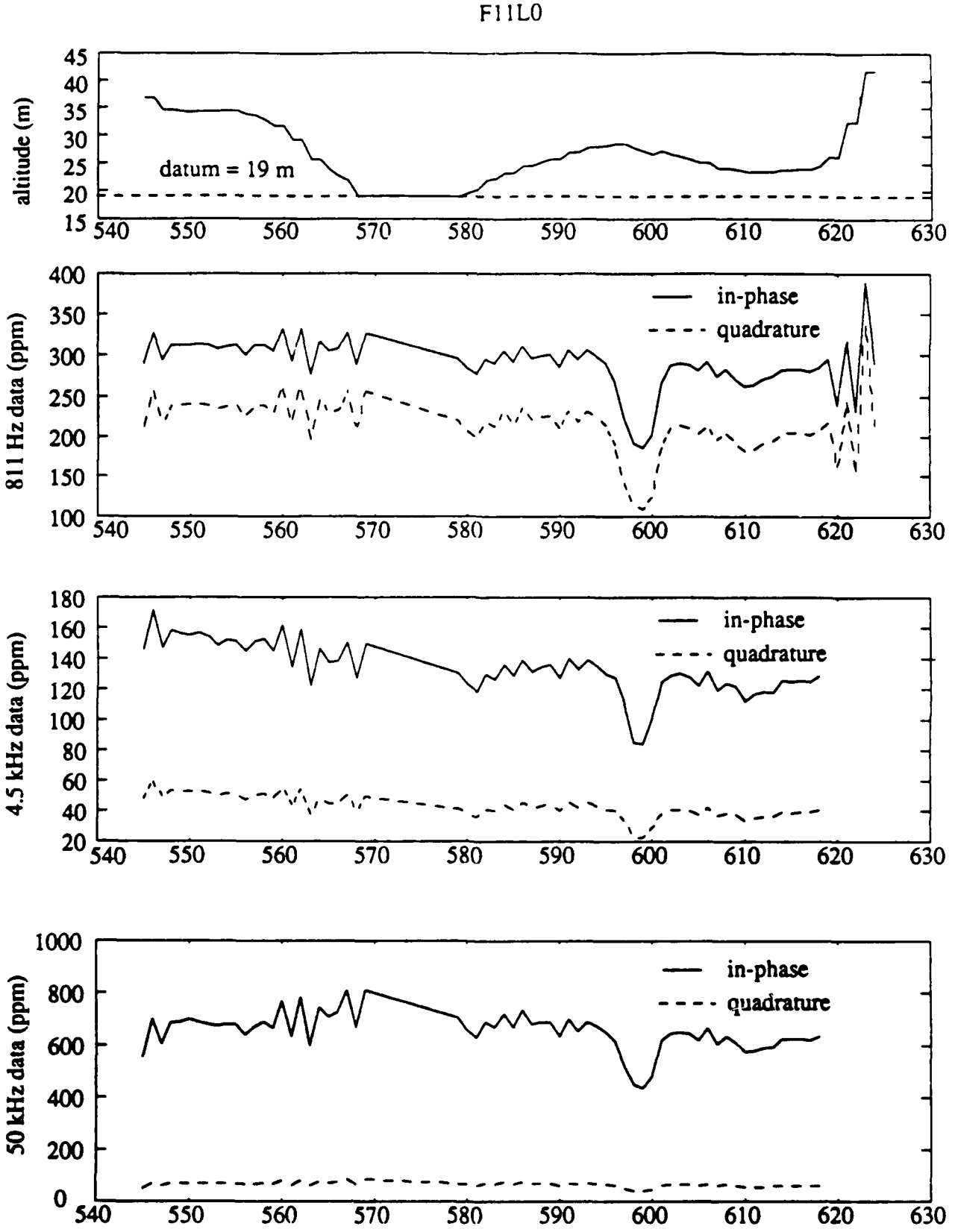

Figure 5. Altitude-corrected data on line F11L0.

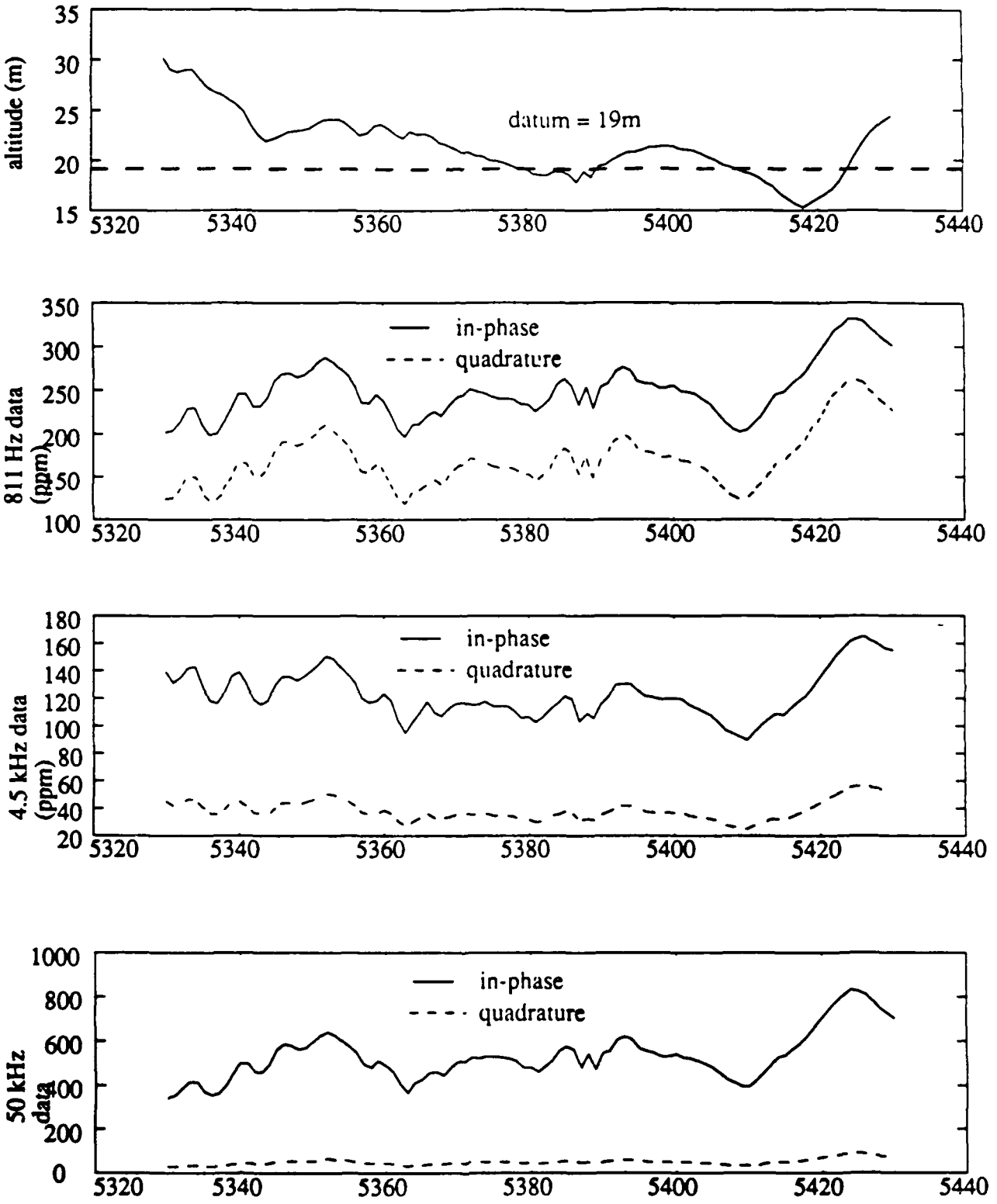

Figure 6. Altitude-corrected data on line F13L8.

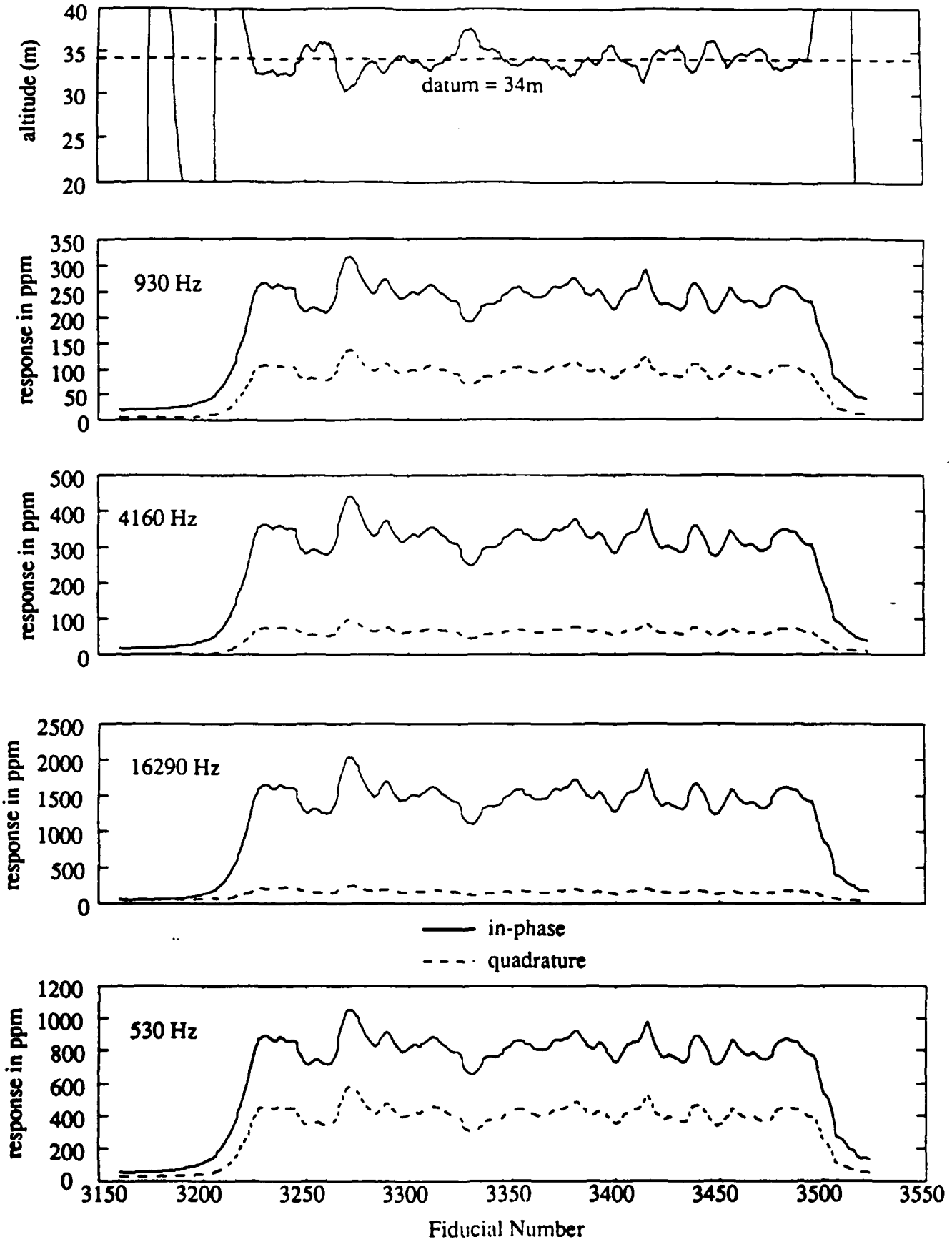

Figure 6(a). Data on line F6L6 collected in 1985. The separation between the transmitter and the receiver is 6.45m.

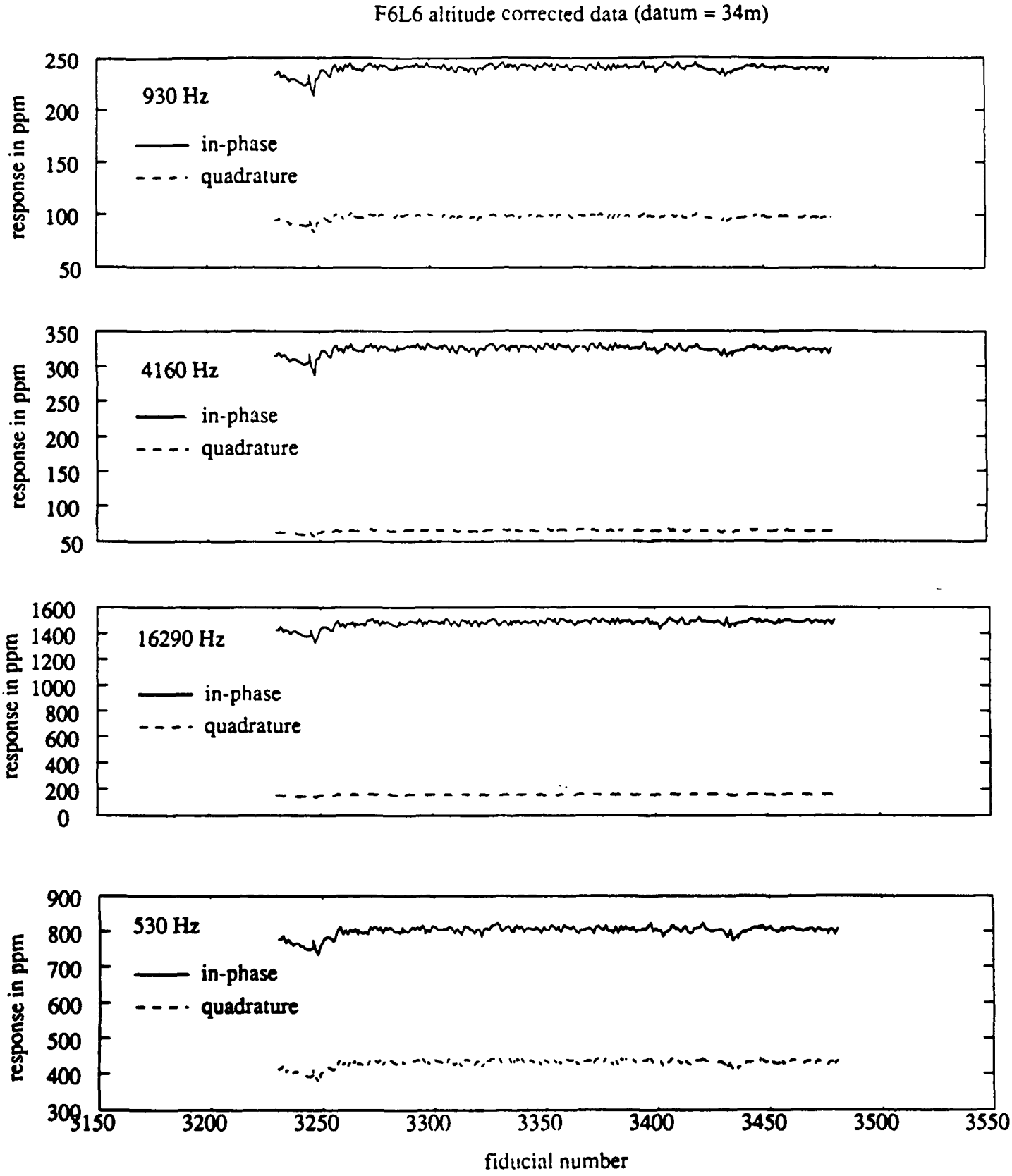

Figure 6(b). Altitude-corrected data on line F6L6.

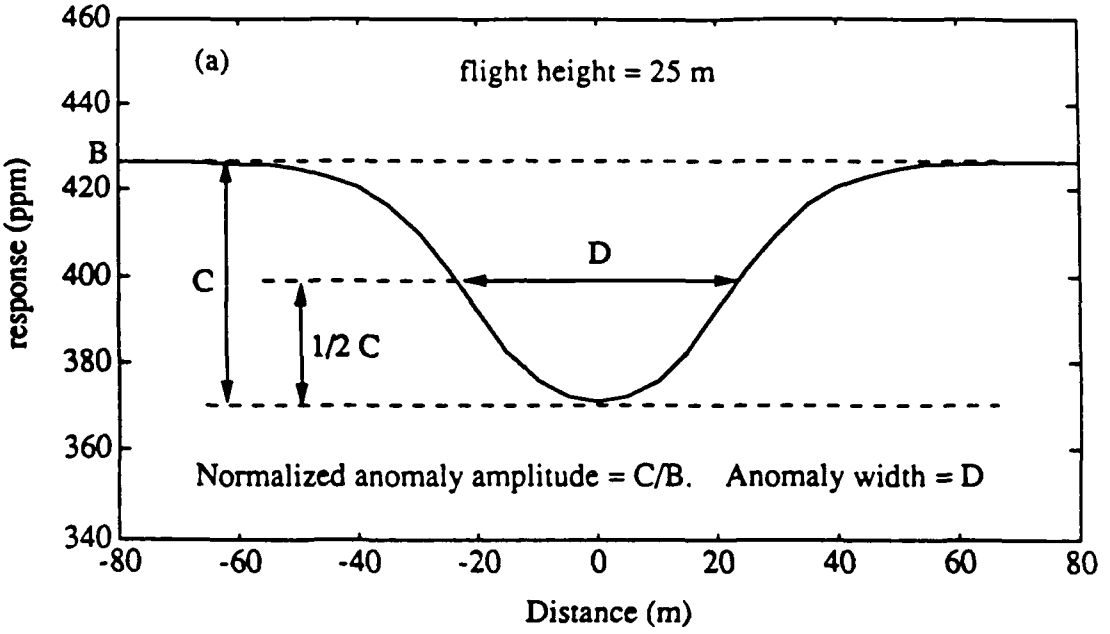

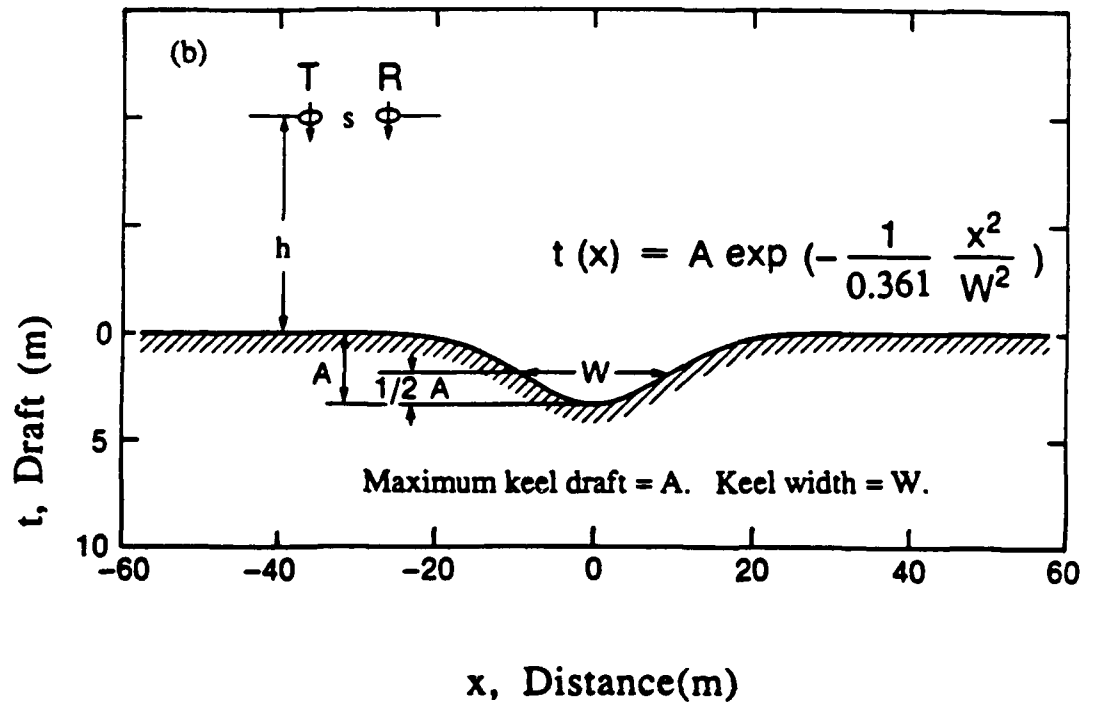

Figure 7. (a) Illustration of anomaly parameters. The system response shown is for the co-planar coil configuration.(b) Illustration of keel parameters. Here, A=3m, W=20m, h=25m, and s=3m.

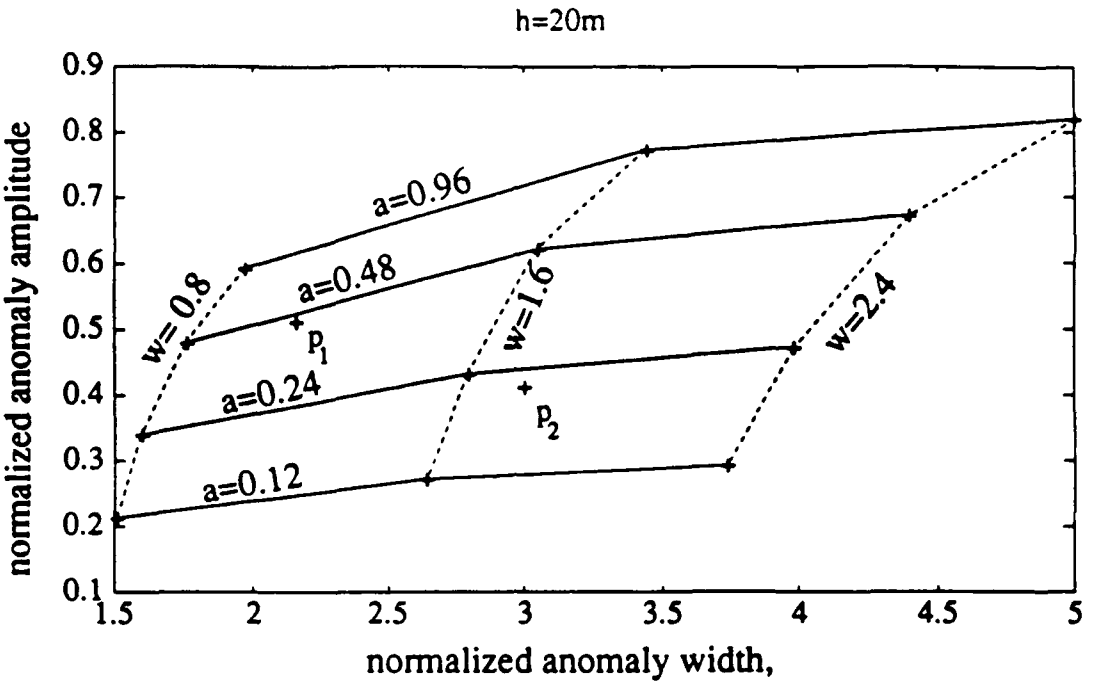

Figure 8. Interpretation chart for the co-axial system; h=20m. The displayed values of a and w are the maximum keel draft and keel width normalized by the bird height h. Points P_1 and P_2 are for anomalies in 4.5 kHz data on lines F14L3 and F11L0.

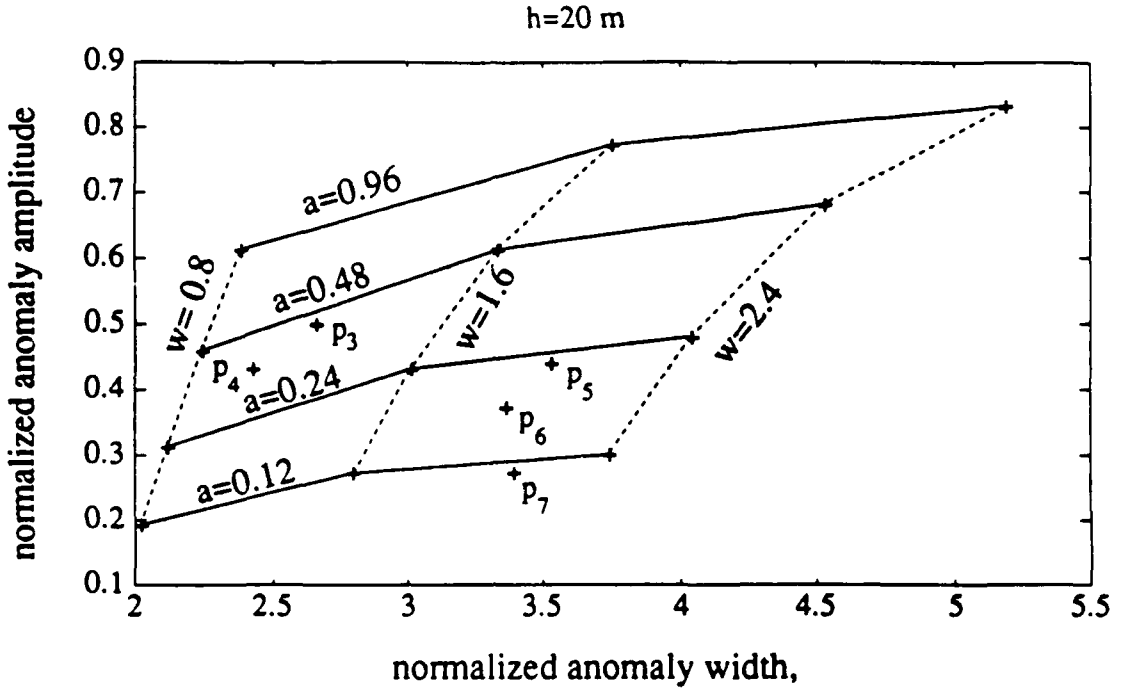

Figure 9. Interpretation chart for the co-planar system; h=20m. Points P_3 and P_4 are for the anomalies in 811 Hz and 50 kHz data in F14L3. Points P_5 and P_6 are for the anomalies in 811 Hz and 50 kHz data in F11L0. Point P_7 is for the 50 kHz data on line F13L8.

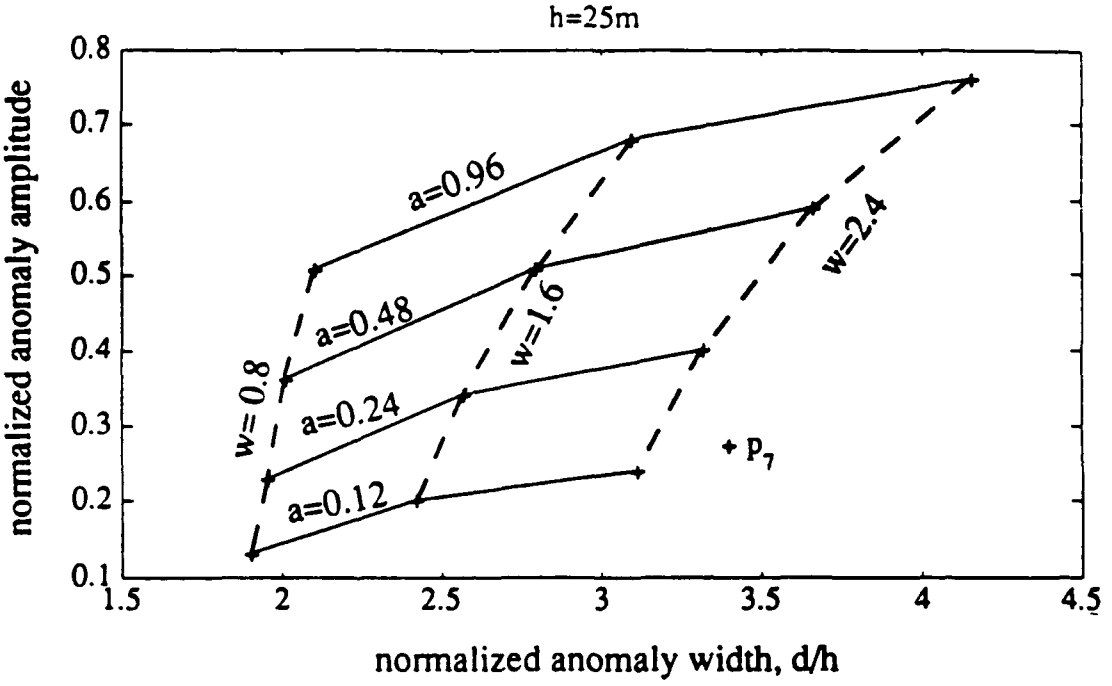

Figure 9(a). Interpretation chart for the co-planar system; h=25m. Point P_7 is for the 50 kHz data on line F13L8.

F14L3

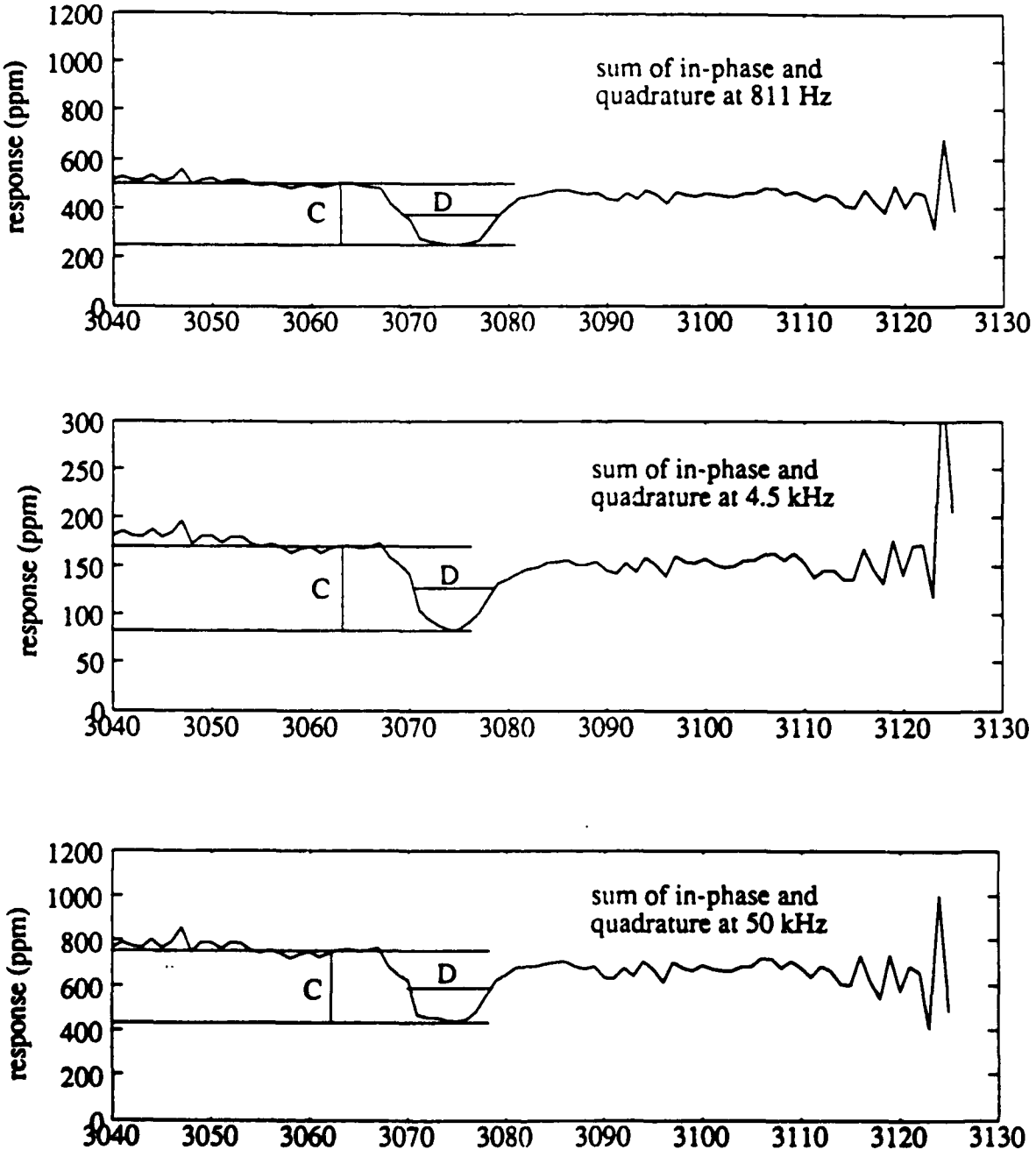

Figure 10. Scaled data and anomaly parameters for line F14L3.

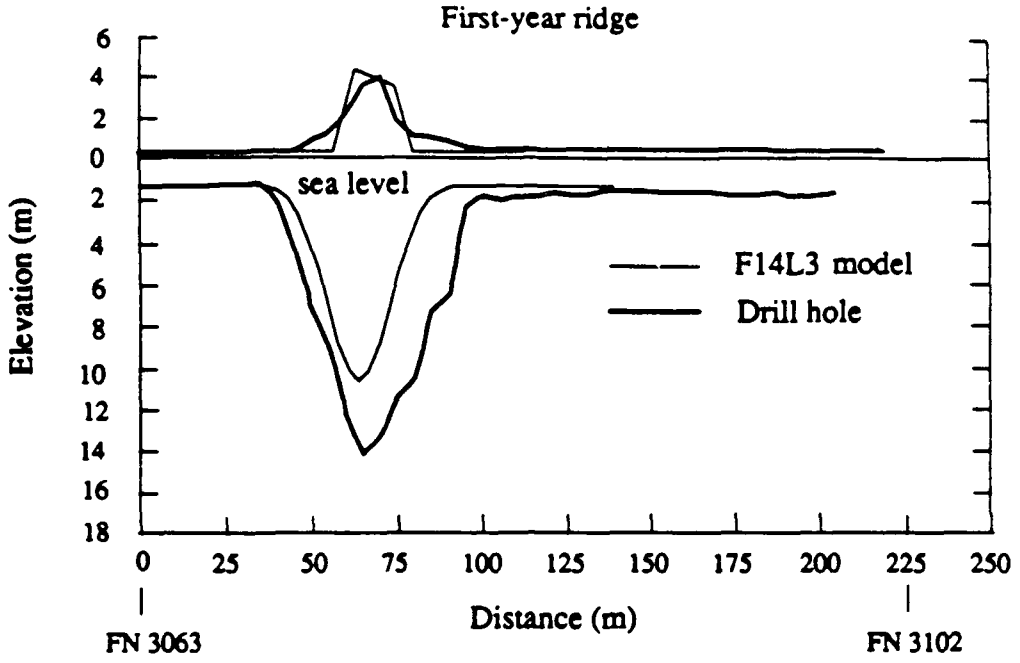

Figure 11. Chart interpretation of the 4.5 kHz data on line F14L3.

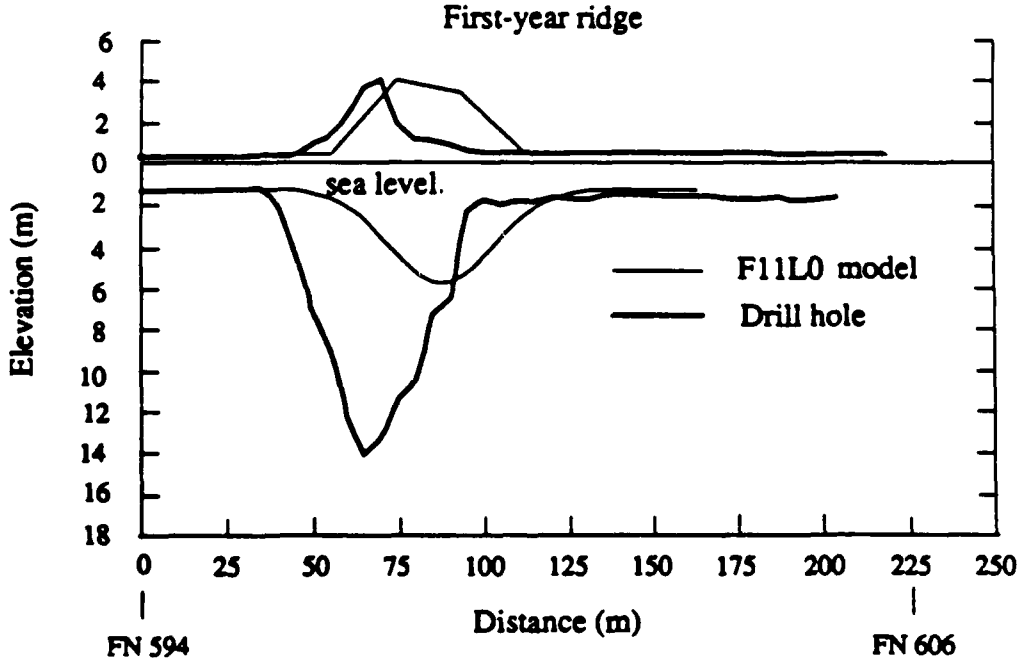

Figure 12. Chart interpretation of the 4.5 kHz data on line F11L0.

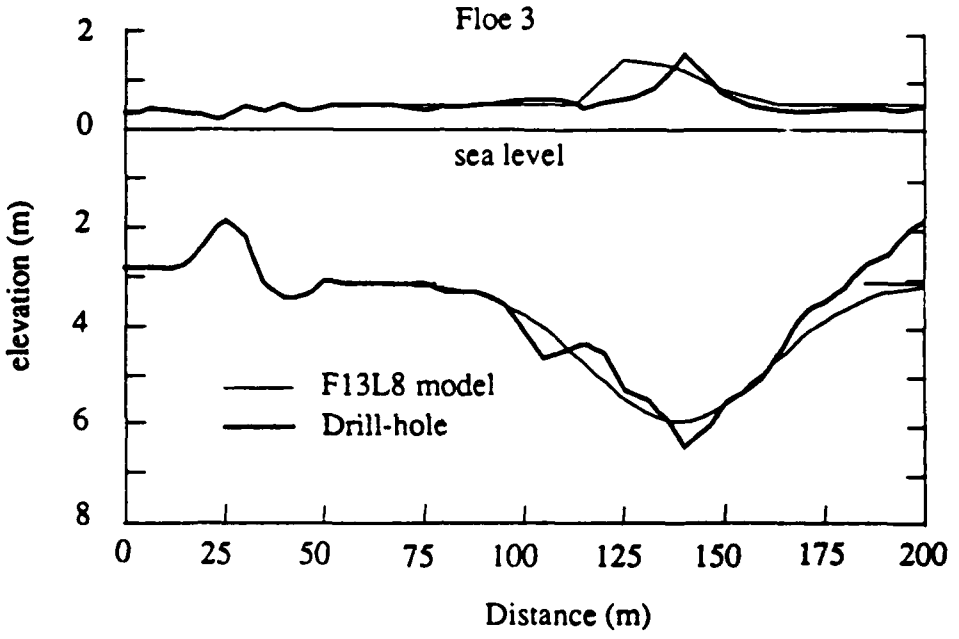

Figure 13. Chart interpretation of the 50 kHz data on line F13L8.

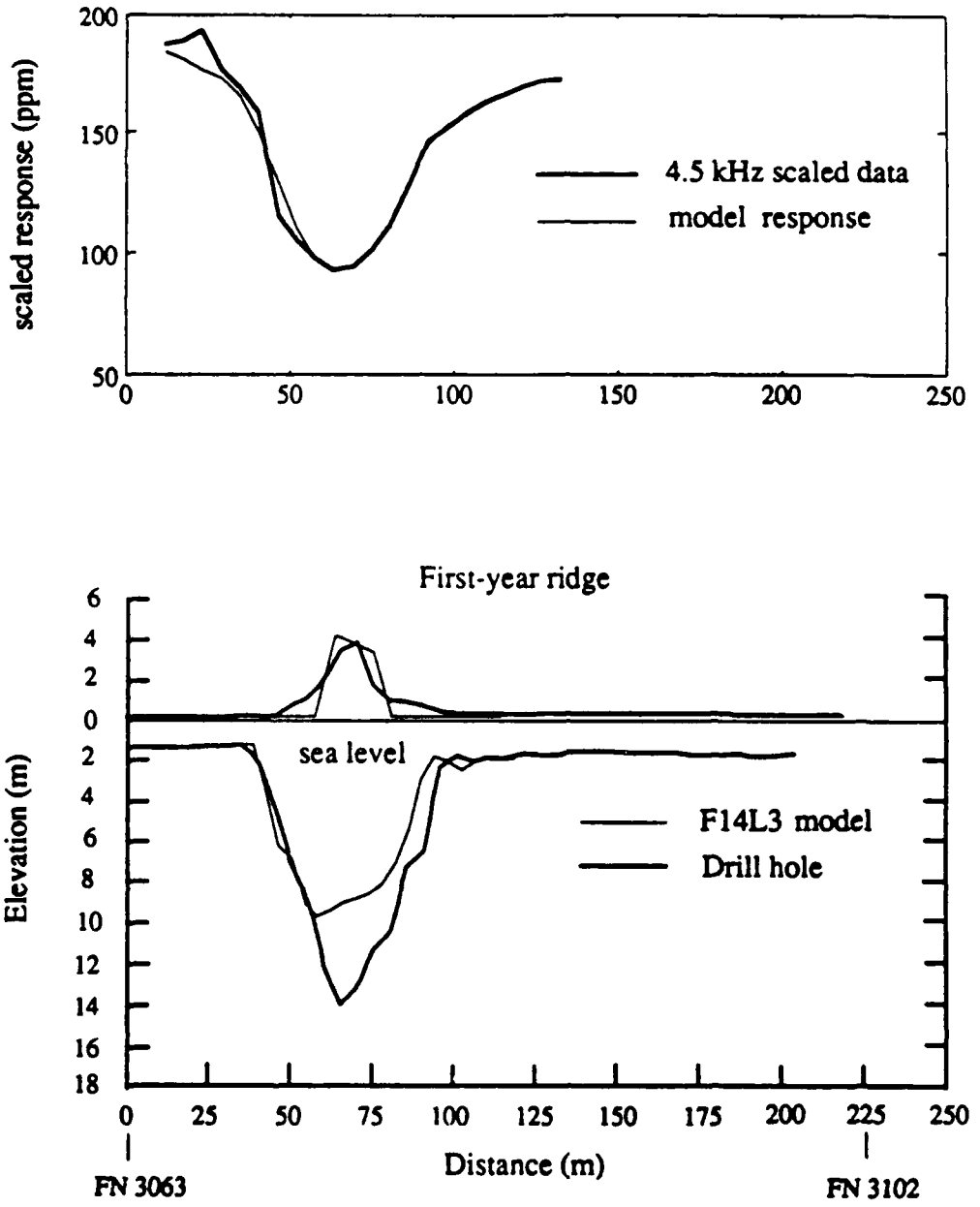

Figure 14. Inversion results of the 4.5 kHz data on line F14L3.

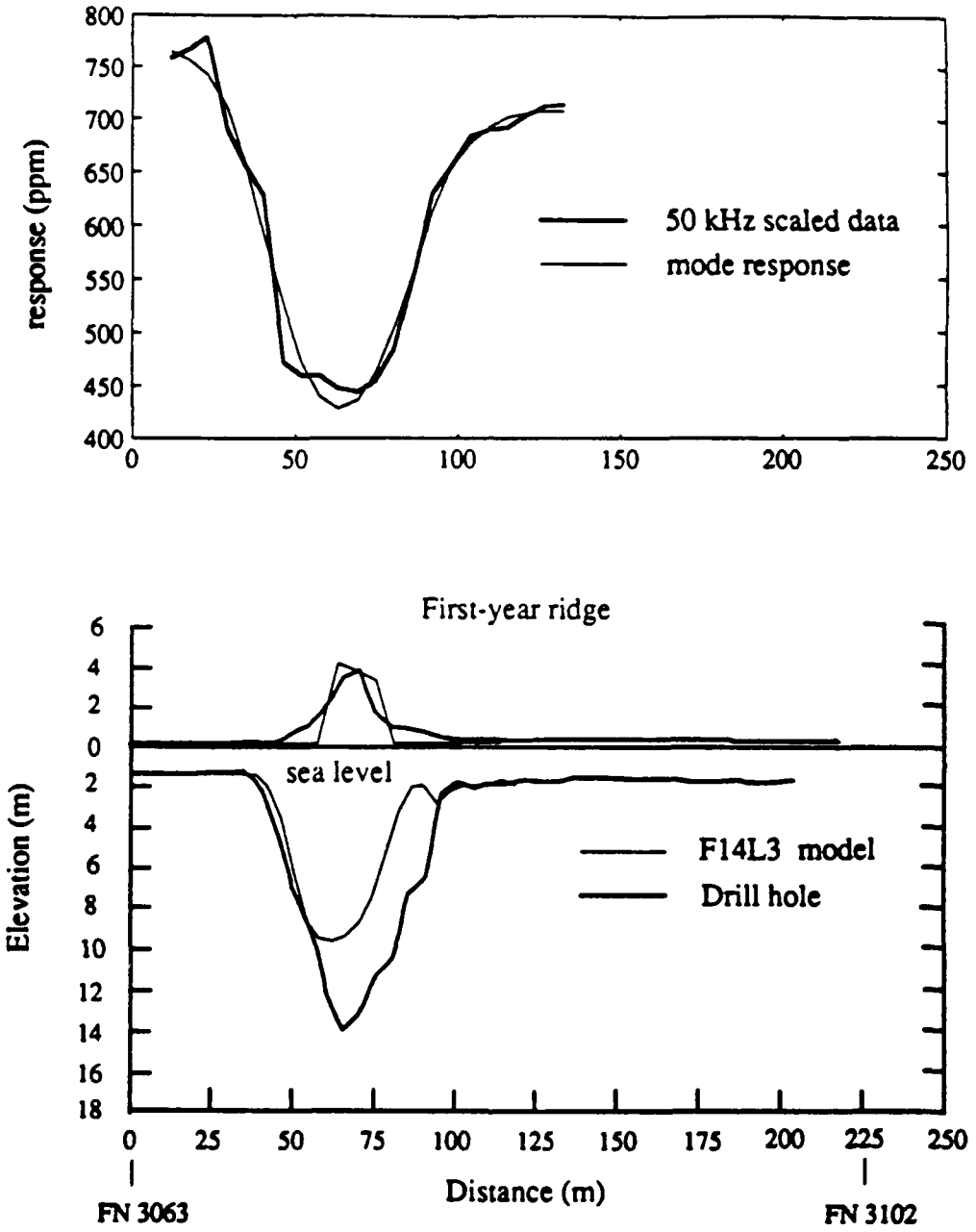

Figure 15. Inversion results of the 50 kHz data on line F14L3.

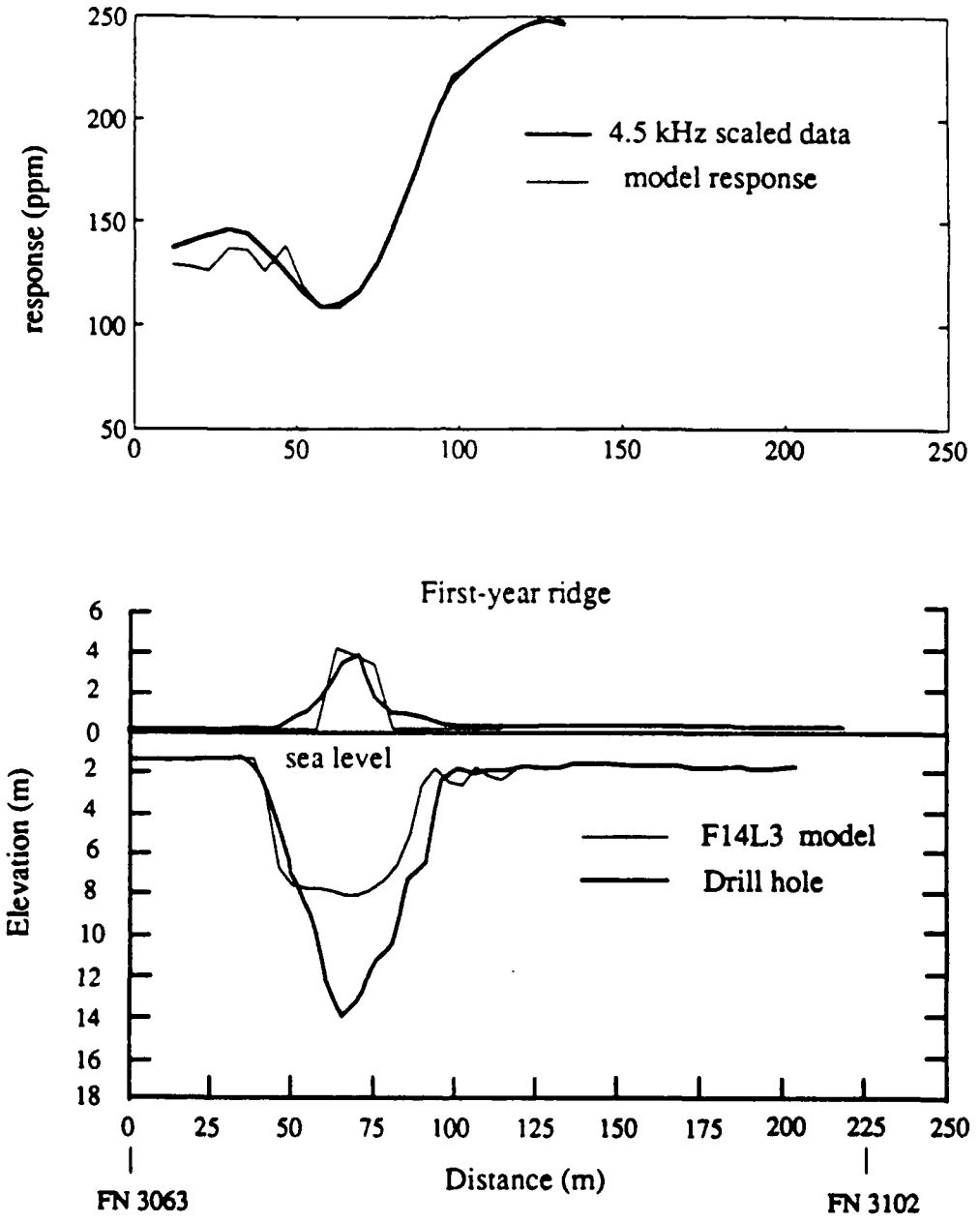

Figure 16. Inversion results of the 4.5 kHz data before altitude correction on line F14L3.

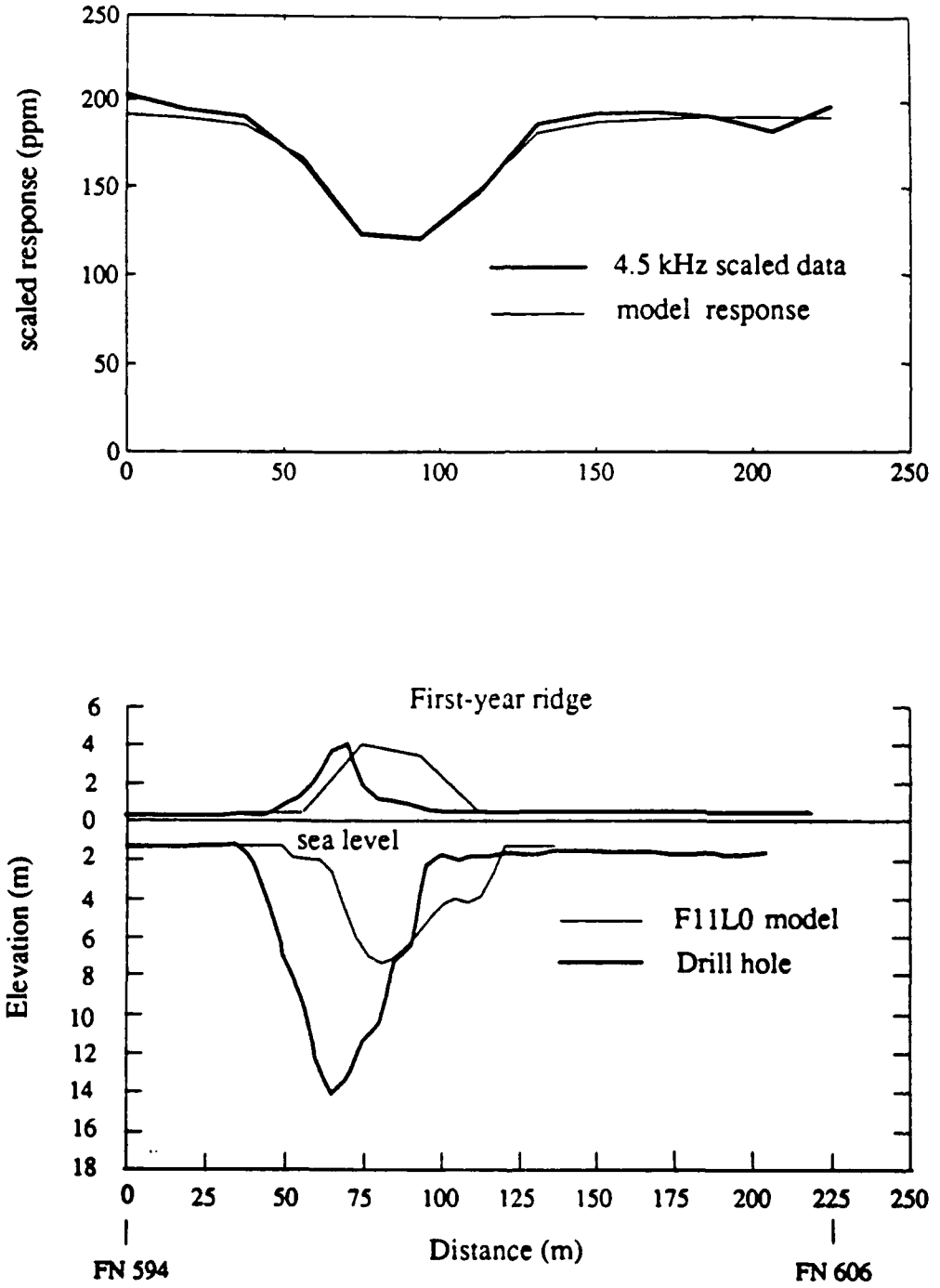

Figure 17. Inversion results of the 4.5 kHz data on line F11L0.

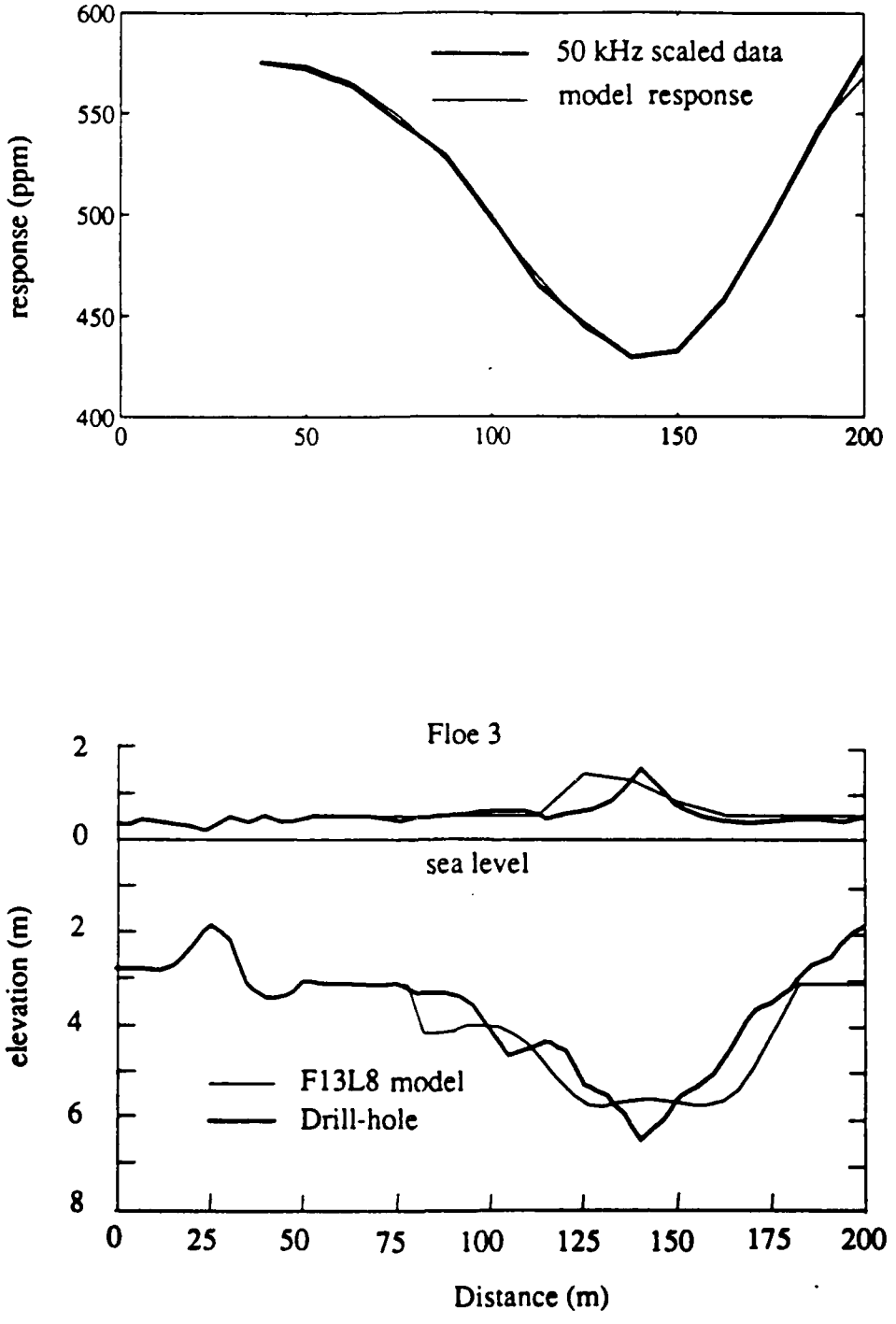

Figure 18. Inversion results of the 50 kHz data on line F13L8.

Appendix Computer Program ALTC for Altitude Correction With Sample Input and Output

```
      program altc2
      dimension alt(200),fid(200),a1(200),a2(200),a3(200)
      dimension b1(200),b2(200),b3(200)
     complex dat1(200),dat2(200),dat3(200),d,hx,hz
      common d,skin1,skin2,skin3,trdis,t2,hx,hz
     common /kk/i
     external func1,func2,func3
     zacc=0.0005
      open (unit=3,file='altc.dat')
      open (unit=4,file='altc.out')
     read(3,*)
      read(3,*) n,f1,f2,f3,trdis,sig,z1,z2,z0
     read(3,*)
    read(3,*) (fid(i),alt(i),a1(i),b1(i),a2(i),b2(i),a3(i),b3(i),
   1  t,t,t,t,i=1,n)
          zm=(z1+z2)/2
    do 20 i=1,n
     dat1(i)=cmplx(a1(i),b1(i))
     dat2(i)=cmplx(a2(i),b2(i))
     dat3(i)=cmplx(a3(i),b3(i))
20    continue
   write(4,10) (fid(i),alt(i),dat1(i),dat2(i),dat3(i),i=1,n)
     skin1=503.292/sqrt(sig*f1)
     skin2=503.292/sqrt(sig*f2)
     skin3=503.292/sqrt(sig*f3)
     t2=trdis**2
     do 100 i=1,n
       d=dat1(i)
                          fbx=func1(zm)
          h=XMIN(z1,zm,z2,FBX,func1,zacc)
       if(i.eq.1) write(4,*) h
         hc=-alt(i)+z0+h
         temp=func1(hc)
       dat1(i)=hz

       d=dat2(i)
         fbx=func2(zm)
          h=XMIN(z1,zm,z2,FBX,func2,zacc)
                              if(i.eq.1) write(4,*) h
         hc=-alt(i)+z0+h
         temp=func2(hc)
       dat2(i)=hx

       d=dat3(i)
         fbx=func3(zm)
          h=XMIN(z1,zm,z2,FBX,func3,zacc)
                              if(i.eq.1) write(4,*) h
         hc=-alt(i)+z0+h
         temp=func3(hc)
       dat3(i)=hz
100  continue
   write(4,10) (fid(i),alt(i),dat1(i),dat2(i),dat3(i),i=1,n)
10   format(2x,'fid  alt(m)     811 Hz      4500 Hz      50000 Hz'
    1 /,(i5,1x,f7.2,3(2x,f7.1,1x,f7.1)))
```

```
      stop
      end

        function func1(he)
         complex d,d2,hz,p,hx
        common /kk/k
         common p,skin1,skin2,skin3,trdis,t2,hx,hz
        d=cmplx(2.*he+skin1,-skin1)
        d2=d**2
        hz=trdis*t2*(2.*d2-t2)/(t2+d2)**2.5*1000000
          if(k.eq.1)  write(4,*) 'hz',hz,'p',p
        func1=cabs(hz-p)
        return
        end

        function func2(he)
         complex d,d2,hx,p,hz
         common p,skin1,skin2,skin3,trdis,t2,hx,hz
        common /kk/k
        d=cmplx(2.*he+skin2,-skin2)
        d2=d*d
        hx=-trdis*t2*(2.*t2-d2)/(t2+d2)**2.5 * 0.5*1000000
          if(k.eq.1)  write(4,*) 'hx',hx,'p',p
        func2=cabs(hx-p)
        return
        end

        function func3(he)
         complex d,d2,hz,p,hx
         common p,skin1,skin2,skin3,trdis,t2,hx,hz
                common /kk/k
        d=cmplx(2.*he+skin3,-skin3)
        d2=d**2
        hz=trdis*t2*(2.*d2-t2)/(t2+d2)**2.5*1000000
                  if(k.eq.1)  write(4,*) 'hz',hz,'p',p
        func3=cabs(hz-p)
        return
        end

      FUNCTION XMIN(AX,BX,CX,FBX,F,TOL)
C XMIN RETURNS the abscissa at which the function is minimum
C
C ON INPUT:
C  AX,BX,CX = INDEPENDENT VARIABLE WHICH BRACKET THE MINIMUM
C  FBX = F(BX) (USUALLY AVAILABLE FROM THE BRACKETING PROCEDURE)
C  F = FUNCTION IN QUESTION
C  TOL = FRACTIONAL TOLERANCE REQUIRED IN THE INDEPENDENT
VARIABLE
C ON OUTPUT:
C  XMIN = ABSCISSA OF MINIMUM
C  FMIN = F(XMIN)
C
C
C
```

```
      PARAMETER (ITMAX=100,CGOLD=.3819660,ZEPS=1.0E - 10)
      A = MIN(AX,CX)
      B = MAX(AX,CX)
      V = BX
      W = V
      X = V
      E = 0.
      FX = FBX
      FV = FX
      FW = FX
      DO 11 ITER = 1,ITMAX
       XM = 0.5*(A + B)
       TOL1 = TOL*ABS(X) + ZEPS
       TOL2 = 2.*TOL1
       IF(ABS(X - XM).LE.(TOL2 - .5*(B - A))) GOTO 3
       IF(ABS(E).GT.TOL1) THEN
        R = (X - W)*(FX - FV)
        Q = (X - V)*(FX - FW)
        P = (X - V)*Q - (X - W)*R
        Q = 2.*(Q - R)
        IF(Q.GT.0.) P =  - P
        Q = ABS(Q)
        ETEMP = E
        E = D
        IF(ABS(P).GE.ABS(.5*Q*ETEMP).OR.P.LE.Q*(A - X).OR.
     *     P.GE.Q*(B - X)) GOTO 1
        D = P/Q
        U = X + D
        IF(U - A.LT.TOL2 .OR. B - U.LT.TOL2) D = SIGN(TOL1,XM - X)
        GOTO 2
       ENDIF
1      IF(X.GE.XM) THEN
        E = A - X
       ELSE
        E = B - X
       ENDIF
       D = CGOLD*E
2      IF(ABS(D).GE.TOL1) THEN
        U = X + D
       ELSE
        U = X + SIGN(TOL1,D)
       ENDIF
       FU = F(U)
       IF(FU.LE.FX) THEN
        IF(U.GE.X) THEN
         A = X
       ELSE
         B = X
       ENDIF
       V = W
       FV = FW
       W = X
       FW = FX
       X = U
```

```
        FX = FU
      ELSE
        IF(U.LT.X) THEN
          A = U
        ELSE
          B = U
        ENDIF
        IF(FU.LE.FW .OR. W.EQ.X) THEN
          V = W
          FV = FW
          W = U
          FW = FU
        ELSE IF(FU.LE.FV .OR. V.EQ.X .OR. V.EQ.W) THEN
          V = U
          FV = FU
        ENDIF
      ENDIF
11    CONTINUE
      WRITE(*,*) 'MAXIMUM ITERATIONS EXCEEDED IN FMIN'
3     XMIN = X
      FMIN = FX
      RETURN
      END
C
```

altc.dat

```
 n  f1  f2  f3   trdis sig  z1   z2   z0
98  811 4500 50000 3.0  2.5   11   60    19
TIME=224944                        LN 0000-

5330 30.09  84.66  40.74  43.71   8.17  120.89   13.25 -3.6 -1.6 4185950 87959901510.
5331 29.01  91.38  45.71  46.30   8.78  135.36   15.87 -5.2 -0.1 4185940 87959301510.
5332 28.64  97.48  50.52  48.80   9.33  148.71   16.69 -4.9 -0.7 4185940 87959301510.
5333 28.89 101.27  52.82  49.37   9.42  153.86   16.54 -3.8 -0.4 4185930 87959101510.
5334 29.00 100.93  52.31  49.18   9.42  152.29   16.02 -3.4 -0.6 4185930 87959101510.
5335 28.07  99.76  52.34  49.60   9.59  152.20   16.17 -3.5 -0.5 4185930 87959101510.
5336 27.31  99.98  53.92  49.95   9.89  156.08   16.13 -3.1 -0.7 4185920 87958501510.
5337 26.81 104.45  56.34  51.42  10.41  165.22   17.19 -2.8 -1.7 4185920 87958501510.
5338 26.42 113.54  62.81  55.86  11.90  186.81   20.17 -2.3 -1.6 4185910 87958001510.
5339 25.98 124.47  71.16  62.85  14.00  214.14   23.29 -1.7 -1.8 4185910 87958001510.
5340 25.59 137.37  79.98  66.57  15.10  240.55   25.96 -1.6 -1.4 4185910 87958001510.
5341 24.75 148.95  85.29  69.16  15.90  259.62   27.22 -1.5 -1.6 4185900 87957501510.
5342 23.45 157.52  89.26  72.96  17.08  276.46   29.37 -1.2 -1.3 4185900 87957501510.
5343 22.46 171.23  99.30  78.73  18.94  309.76   33.04 -1.2 -0.2 4185890 87957101510.
5344 21.86 187.65 112.66  85.99  21.45  350.76   37.89 -1.0 -1.1 4185890 87957101510.
5345 22.09 198.39 121.83  90.81  23.20  381.84   42.89 -0.9 -0.3 4185890 87957101510.
5346 22.40 198.63 121.73  91.44  23.35  381.89   42.02 -0.8 -0.1 4185870 87956601510.
5347 22.79 193.55 116.28  87.86  21.98  363.60   39.02 -0.8 -0.7 4185870 87956601510.
5348 22.83 189.63 112.21  85.40  21.11  350.30   36.80 -0.7 -0.5 4185870 87956201510.
5349 22.99 188.50 111.64  85.94  21.53  350.44   36.88 -0.2 -1.0 4185870 87956201510.
5350 23.18 189.48 112.73  85.96  21.55  355.38   38.18  0.2 -1.5 4185870 87956201510.
5351 23.60 188.27 111.19  84.90  21.29  353.08   38.06  0.5 -1.4 4185860 87955701510.
5352 24.00 184.56 108.63  83.67  20.93  344.84   36.68  0.5 -1.8 4185860 87955701510.
5353 24.11 179.58 104.97  81.79  20.44  333.09   35.02  0.9 -1.1 4185850 87955301510.
5354 24.04 176.67 102.56  79.85  19.82  325.17   33.81  0.5 -1.4 4185850 87955301510.
5355 23.66 176.73 103.98  80.53  20.10  328.69   35.17  0.1 -1.3 4185850 87955301510.
```

5356	23.08	176.73	106.61	82.16	20.79	334.65	35.99	0.3	-0.9	4185830	87954701510.
5357	22.45	172.58	104.72	81.26	20.29	329.79	36.98	-0.1	-0.1	4185830	87954701510.
5358	22.69	168.70	100.26	77.29	19.27	312.59	33.78	-0.8	-0.8	4185830	87954501510.
5359	23.40	165.61	98.24	72.64	17.28	304.37	33.03	-1.0	-0.8	4185830	87954501510.
5360	23.54	156.59	94.82	74.16	17.81	291.44	31.77	-0.2	0.2	4185830	87954501510.
5361	23.20	150.29	93.19	74.22	17.88	283.81	30.68	-0.7	-1.5	4185810	87953801510.
5362	22.55	147.13	89.72	70.75	16.67	271.48	28.71	-0.3	-0.5	4185810	87953801510.
5363	22.16	146.59	86.58	67.73	15.55	259.55	26.23	-0.7	-0.7	4185800	87953501510.
5364	22.83	148.57	88.69	68.57	15.82	266.87	27.62	-0.6	-2.3	4185800	87953501510.
5365	22.54	150.87	93.69	74.10	18.06	284.06	31.02	-0.3	-0.6	4185800	87953501510.
5366	22.64	155.82	98.09	78.13	19.80	299.71	33.48	-0.4	-1.7	4185790	87952901510.
5367	22.39	163.70	102.04	75.56	18.69	310.72	32.99	-0.6	-1.6	4185790	87952901510.
5368	21.81	168.96	104.44	78.52	19.96	320.76	34.67	-0.9	-1.0	4185780	87952501510.
5369	21.56	180.97	114.57	84.54	21.99	353.75	38.90	-1.1	-0.6	4185780	87952501510.
5370	21.14	195.06	125.48	91.00	24.38	388.95	43.06	-0.6	-0.8	4185780	87952501510.
5371	20.80	205.51	130.97	95.13	25.78	408.83	44.70	-0.7	-0.7	4185770	87952001510.
5372	20.74	214.70	135.63	94.75	25.30	423.09	45.32	-0.9	-0.6	4185770	87952001510.
5373	20.51	217.40	137.36	96.86	26.21	430.14	45.99	-0.4	-0.6	4185760	87951601510.
5374	20.38	216.86	139.44	100.18	28.15	442.32	50.47	-0.3	-0.3	4185760	87951601510.
5375	20.01	218.99	144.45	101.73	29.00	463.62	55.49	-0.5	-1.8	4185760	87951601510.
5376	19.83	220.65	146.40	103.68	29.98	470.11	56.75	-0.4	-1.0	4185750	87951101510.
5377	19.63	224.22	149.78	106.29	30.62	476.39	55.31	-0.6	-1.0	4185750	87951101510.
5378	19.36	228.66	153.45	106.65	30.35	483.54	53.92	-0.7	-1.6	4185740	87950701510.
5379	19.09	230.18	152.32	104.67	29.24	473.88	50.77	-0.8	-1.1	4185740	87950701510.
5380	19.15	228.50	150.44	104.85	29.24	467.65	49.49	-0.6	-0.9	4185740	87950701510.
5381	18.60	231.49	153.95	107.16	30.22	481.71	51.67	-0.7	-1.9	4185720	87950201510.
5382	18.52	239.92	162.77	112.58	32.70	512.95	57.51	0.1	-0.8	4185720	87950201510.
5383	18.51	250.26	170.66	118.51	35.22	542.11	61.86	-0.5	-0.3	4185710	87949801510.
5384	18.84	262.21	177.23	118.33	35.21	563.88	63.57	-0.1	-0.7	4185710	87949801510.

5385	18.88	267.67	182.09	123.67	37.77	580.70	65.80	0.2	-0.8	4185710	87949801510.
5386	18.58	265.93	182.80	125.88	37.94	588.05	67.63	0.2	-1.3	4185700	87949301510.
5387	17.76	262.53	175.46	119.63	35.39	557.73	61.34	0.1	-0.4	4185700	87949301510.
5388	18.87	259.87	172.20	110.98	31.42	547.34	59.14	-0.1	-0.8	4185700	87949001510.
5389	18.25	247.06	161.56	115.59	34.01	512.67	55.21	0.1	-1.5	4185700	87949001510.
5390	19.41	246.56	162.43	110.79	31.46	512.42	54.69	0.2	-0.8	4185700	87949001510.
5391	19.58	246.38	162.59	113.53	33.20	514.65	55.22	0.1	-0.7	4185680	87948401510.
5392	20.08	246.78	164.01	113.56	33.12	521.32	56.04	0.1	-1.7	4185680	87948401510.
5393	20.48	243.69	159.58	109.08	31.20	507.40	53.27	0.7	-1.3	4185670	87948001510.
5394	20.76	233.93	150.02	105.69	30.00	480.36	49.90	0.8	-0.9	4185670	87948001510.
5395	20.75	224.28	141.35	101.96	28.61	452.78	46.05	1.3	-1.4	4185670	87948001510.
5396	21.01	217.24	134.48	96.53	26.25	428.63	42.40	1.7	-0.3	4185660	87947301510.
5397	21.31	211.62	128.91	92.53	24.46	409.99	39.75	1.9	-1.0	4185660	87947301510.
5398	21.32	207.52	125.24	91.32	24.09	397.21	38.22	1.8	-0.4	4185650	87947101510.
5399	21.35	206.45	125.22	90.77	24.00	396.70	37.78	1.7	-0.5	4185650	87947101510.
5400	21.35	207.67	127.34	91.58	24.29	403.46	38.99	1.6	-0.8	4185650	87947101510.
5401	21.06	207.79	127.54	93.95	25.57	405.31	39.14	1.8	-0.9	4185640	87946801510.
5402	20.93	209.32	128.51	92.18	24.57	409.58	40.31	2.4	-1.0	4185640	87946801510.
5403	20.86	209.31	128.02	91.27	24.16	406.90	39.70	2.2	-1.8	4185630	87946101510.
5404	20.62	207.66	128.62	92.15	24.58	406.20	39.48	1.9	-0.6	4185630	87946101510.
5405	20.31	206.45	130.64	92.89	24.86	409.69	39.77	1.6	-1.0	4185630	87946101510.
5406	19.94	203.37	130.42	92.88	24.81	405.68	39.53	1.6	-1.1	4185620	87945701510.
5407	19.51	199.65	129.23	91.63	24.26	398.76	38.65	1.6	-0.7	4185620	87945701510.
5408	19.28	196.15	127.80	91.61	24.20	393.03	38.64	1.3	-1.5	4185610	87945301510.
5409	19.04	196.31	127.53	91.63	24.17	389.33	37.45	1.6	-1.1	4185610	87945301510.
5410	18.81	202.68	132.63	92.08	23.99	403.05	38.90	1.7	-0.3	4185610	87945301510.
5411	18.57	214.73	143.19	100.02	27.21	438.90	43.44	1.8	-0.6	4185590	87944701510.
5412	18.13	234.51	161.01	111.64	32.37	501.41	51.88	1.8	-0.8	4185590	87944701510.
5413	17.69	260.40	182.55	122.78	37.19	578.84	63.81	1.5	-0.8	4185580	87944301510.

5414	17.26	289.89	204.90	134.08	42.22	658.13	76.05	1.2	-0.7	4185580	87944301510.
5415	16.55	319.24	227.77	146.27	47.54	741.10	89.61	1.1	-1.1	4185580	87944301510.
5416	16.08	348.96	254.40	162.86	54.97	833.84	104.74	1.0	-1.2	4185570	87943701510.
5417	15.57	380.99	286.71	182.55	64.17	950.71	126.49	1.4	-0.7	4185570	87943701510.
5418	15.29	409.68	315.92	198.59	71.90	1059.30	147.96	1.4	-1.4	4185560	87943301510.
5422	16.95	412.23	314.56	198.00	71.54	1058.83	147.46	0.9	-1.8	4185550	87942901510.
5423	17.91	380.10	281.64	179.65	62.68	940.68	123.02	0.9	-0.7	4185540	87942501510.
5424	19.11	342.20	243.82	158.70	53.00	810.32	98.92	1.0	0.3	4185540	87942501510.
5425	20.35	302.41	204.60	136.95	43.29	677.53	76.21	1.0	-2.1	4185540	87942501510.
5426	21.60	265.88	170.46	118.22	35.36	563.80	59.49	1.0	-0.3	4185530	87941901510.
5427	22.53	238.18	146.03	104.41	29.89	482.88	48.02	0.9	-0.2	4185530	87941901510.
5428	23.31	217.02	128.12	94.29	25.89	425.43	41.03	1.8	-2.0	4185520	87941601510.
5429	23.92	201.83	115.83	86.86	23.05	385.38	36.86	2.6	-0.3	4185520	87941601510.
5430	24.33	191.36	107.40	82.13	21.35	357.53	33.00	2.9	-0.5	4185520	87941601510.

altc.out

fid	alt(m)	811 Hz		4500 Hz		50000 Hz	
5330	30.09	201.5	123.6	138.6	44.8	338.8	26.7
5331	29.01	202.8	124.8	131.2	41.6	351.7	28.0
5332	28.64	213.7	134.8	134.6	43.1	383.6	31.5
5333	28.89	228.6	149.0	141.3	46.0	413.6	34.8
5334	29.00	229.5	149.8	142.6	46.6	412.5	34.7
5335	28.07	209.7	131.1	128.4	40.4	370.2	30.0
5336	27.31	198.3	120.8	118.2	36.1	351.6	28.0
5337	26.81	199.4	121.7	115.8	35.1	358.1	28.7
5338	26.42	212.7	133.9	123.1	38.1	401.1	33.4
5339	25.98	228.1	148.4	135.6	43.5	453.5	39.4
5340	25.59	245.7	165.9	138.8	44.9	500.8	44.9
5341	24.75	246.3	166.4	130.9	41.5	496.4	44.4
5342	23.45	231.2	151.5	118.9	36.4	456.3	39.7
5343	22.46	231.1	151.3	115.3	34.9	461.0	40.2
5344	21.86	241.1	161.2	118.4	36.2	492.7	44.0
5345	22.09	260.9	181.5	129.4	40.8	558.5	52.0
5346	22.40	268.5	189.5	135.5	43.5	581.6	54.9
5347	22.79	269.9	191.0	136.0	43.7	577.9	54.4
5348	22.83	264.6	185.4	132.2	42.1	556.2	51.7
5349	22.99	267.0	187.9	136.1	43.8	568.2	53.2
5350	23.18	273.5	194.9	139.5	45.2	592.7	56.3
5351	23.60	281.9	204.1	144.9	47.7	622.6	60.1
5352	24.00	286.6	209.3	150.1	50.0	638.2	62.1
5353	24.11	281.5	203.6	148.2	49.1	621.1	59.9
5354	24.04	274.6	196.0	142.7	46.7	597.4	56.9
5355	23.66	266.5	187.4	137.5	44.4	575.4	54.1
5356	23.08	254.9	175.3	130.9	41.5	545.4	50.4
5357	22.45	235.8	156.0	119.5	36.6	495.0	44.2
5358	22.69	234.3	154.4	116.4	35.4	479.3	42.4
5359	23.40	245.1	165.3	117.8	35.9	507.7	45.8
5360	23.54	236.5	156.7	122.8	38.0	490.7	43.7
5361	23.20	222.2	142.7	118.0	36.0	456.5	39.7
5362	22.55	204.5	126.3	103.5	30.1	401.5	33.5
5363	22.16	195.3	118.1	94.1	26.5	364.7	29.4
5364	22.83	210.1	131.5	103.0	29.9	406.7	34.1
5365	22.54	210.6	131.9	109.0	32.3	422.3	35.8
5366	22.64	220.2	140.9	117.3	35.7	454.2	39.4
5367	22.39	225.1	145.5	109.5	32.6	458.7	40.0
5368	21.81	219.9	140.6	107.0	31.5	443.2	38.2
5369	21.56	231.0	151.2	112.5	33.7	478.9	42.3
5370	21.14	239.5	159.7	116.1	35.2	504.5	45.4
5371	20.80	242.8	162.9	116.7	35.5	510.3	46.1
5372	20.74	250.3	170.5	115.3	34.9	525.0	47.9
5373	20.51	247.9	168.0	114.9	34.7	519.1	47.1
5374	20.38	246.0	166.1	117.5	35.8	526.4	48.0
5375	20.01	242.0	162.1	114.3	34.5	527.9	48.2
5376	19.83	240.2	160.3	114.2	34.4	523.5	47.7
5377	19.63	239.8	159.9	114.3	34.5	517.2	46.9
5378	19.36	238.5	158.6	110.9	33.1	507.4	45.7
5379	19.09	232.9	153.1	105.3	30.9	480.5	42.5
5380	19.15	232.2	152.5	106.3	31.2	477.5	42.2
5381	18.60	224.5	145.0	101.9	29.5	459.9	40.1
5382	18.52	231.3	151.5	106.0	31.1	484.1	43.0
5383	18.51	239.5	159.6	111.4	33.3	510.7	46.1
5384	18.84	255.5	175.9	115.8	35.1	553.3	51.3

5385	18.88	261.5	182.1	121.7	37.6	572.7	53.7
5386	18.58	254.2	174.5	119.2	36.5	558.0	51.9
5387	17.76	231.6	151.8	102.9	29.9	477.6	42.2
5388	18.87	252.8	173.0	108.7	32.2	539.3	49.6
5389	18.25	228.6	148.9	105.4	30.9	467.6	41.0
5390	19.41	253.7	174.0	115.8	35.1	541.3	49.8
5391	19.58	257.6	178.1	121.3	37.4	555.3	51.6
5392	20.08	270.7	191.9	129.0	40.7	601.1	57.3
5393	20.48	276.2	197.9	130.0	41.1	616.2	59.2
5394	20.76	271.7	193.0	130.2	41.2	602.7	57.5
5395	20.75	259.9	180.5	125.0	39.0	565.1	52.8
5396	21.01	257.6	178.1	121.7	37.6	551.0	51.0
5397	21.31	257.2	177.6	120.4	37.0	545.9	50.4
5398	21.32	252.3	172.6	118.8	36.4	527.2	48.1
5399	21.35	251.9	172.2	118.6	36.3	528.5	48.3
5400	21.35	254.3	174.6	119.7	36.7	539.0	49.6
5401	21.06	247.9	168.1	119.0	36.4	521.5	47.4
5402	20.93	246.7	166.8	114.6	34.6	518.7	47.1
5403	20.86	244.8	165.0	112.5	33.7	510.7	46.1
5404	20.62	238.9	159.1	110.5	32.9	495.5	44.3
5405	20.31	232.9	153.1	107.5	31.7	480.8	42.6
5406	19.94	223.5	144.0	102.9	29.9	453.9	39.4
5407	19.51	212.3	133.5	96.6	27.4	424.1	36.0
5408	19.28	205.4	127.2	94.1	26.5	407.0	34.1
5409	19.04	201.2	123.4	91.6	25.5	392.0	32.4
5410	18.81	203.2	125.2	89.6	24.8	394.9	32.7
5411	18.57	210.4	131.7	94.8	26.8	417.7	35.3
5412	18.13	220.1	140.8	100.6	29.0	451.3	39.1
5413	17.69	232.3	152.5	104.8	30.7	490.6	43.7
5414	17.26	244.0	164.1	108.4	32.1	524.4	47.8
5415	16.55	247.3	167.4	108.1	32.0	533.4	48.9
5416	16.08	255.1	175.4	112.6	33.8	557.4	51.8
5417	15.57	262.4	183.1	117.1	35.7	584.2	55.2
5418	15.29	271.4	192.7	121.7	37.6	617.1	59.4
5422	16.95	316.9	244.3	149.5	49.8	777.6	80.8
5423	17.91	323.8	252.6	154.7	52.1	800.8	84.0
5424	19.11	330.2	260.4	160.7	54.9	825.9	87.6
5425	20.35	330.7	261.1	162.8	55.9	823.4	87.2
5426	21.60	328.0	257.8	164.1	56.5	809.0	85.2
5427	22.53	320.4	248.5	161.5	55.3	775.9	80.6
5428	23.31	313.2	239.8	158.9	54.1	746.3	76.5
5429	23.92	307.4	233.0	156.0	52.7	721.8	73.2
5430	24.33	301.3	226.0	154.0	51.8	696.4	69.8